BIRL
Industrial Research Laboratory
Northwestern University
1801 Maple Avenue
Evanston, Illinois 60201-3135

Contract No. NAS 8-37686

FINAL REPORT

APPLICATION OF HARD COATINGS TO SUBSTRATES AT LOW TEMPERATURES

FOR

NASA MARSHALL SPACE FLIGHT CENTER

by

William D. Sproul
Group Leader

June 15, 1993

TABLE OF CONTENTS

LIST OF FIGURES

LIST OF TABLES

EXECUTIVE SUMMARY

BIRL, the industrial research laboratory of Northwestern University, has conducted unique and innovative research, under sponsorship [1] from the NASA Marshall Space Flight Center (MSFC), in the application of hard, wear resistant coatings to bearing steels using the high-rate reactive sputtering (HRRS) process that was pioneered by Dr. William Sproul [2], the principal investigator on this program. Prior to this program, Dr. Sproul had demonstrated [2-5] that it is possible to apply hard coatings such as titanium nitride (TiN) to alloy steels at low temperatures via the HRRS process without changing the metallurgical properties of the steel. The NASA MSFC program at BIRL had the specific objectives to:

- Apply TiN to 440C stainless steel without changing the metallurgical properties of the steel
- Prepare rolling contact fatigue (RCF) test samples coated with binary hard coatings of TiN, zirconium nitride (ZrN), hafnium nitride (HfN), chromium nitride (CrN), and molybdenum nitride (MoN), and metal coatings of copper (Cu) and gold (Au)
- Develop new alloyed hard coatings of titanium aluminum nitride ($Ti_{0.5}Al_{0.5}N$), titanium zirconium nitride ($Ti_{0.5}Zr_{0.5}N$), and titanium aluminum vanadium nitride ([Ti-Al-V]N).

Overall, the objectives of the NASA MSFC program have been successfully met. All of the nitride coatings were synthesized using the HRRS process to control the composition of the coatings, and both the nitride and pure metal coatings were deposited on RCF test rods using the unbalanced magnetron (UBM) sputtering process. Details of the UBM coating process, results of the coating characterization, and results from the RCF tests are given in the main body of this report.

All of the coatings were deposited on the RCF test rods at four different coatings thicknesses of 0.25, 0.50, 0.75, and 1.00 μm. All of the nitride coatings produced improvements in the RCF life in tests carried out at MSFC, and six of the eight coatings gave significant enhancements in RCF life. Usually the greatest improvement in RCF life was for coatings with a thickness of 0.50 to 0.75 μm. The largest improvement in RCF life was exhibited by the 0.5 μm thick HfN coating at both the 4.0 and 5.4 GPa test stress levels where the HfN coated specimens had a 12 to 13 fold improvement in RCF life compared to an uncoated specimen. The pure metal coatings were still under test at the time of this writing, but preliminary results indicate even larger improvements than the hard coatings at 4.0 GPa. Results of Au and Cu coated specimens at 5.4 GPa do not show significant improvements over uncoated specimens.

Over the course of this program, several papers have been published on the progress of the coating and RCF work. This final report brings together all of the work in one volume. Excerpts from some of the papers have been used in compiling this final report.

UNBALANCED MAGNETRON SPUTTERING

Sputter Coating

Sputter coating of large three dimensional parts such as gear cutting hobs or an injection molding screw presents special problems. Sputtering is basically a line of sight process, and if a single sputtering target is used, a large object to be coated requires substrate rotation. Since only one side of the part faces the sputtering target in a single target system at any given time, half of the part will be in the shadow of the sputtered flux. Only highly scattered atoms reach the shadowed side of the part, and they arrive with very little energy.

The quality of the coating is questionable in the shadowed area, and reactive sputtering exacerbates the problem even more. The arrival of the metal species in the shadowed area is by scattering only, whereas the nonmetal gaseous species is present in the same amount nominally on all sides of the

part. This effect means that the compound formed in the shadow, although very thin, will be highly over stoichiometric, and as the part rotates, a layered structure of stoichiometric and over-stoichiometric coating will be formed.

Multiple cathode sputtering systems can alleviate the shadowing problem. Opposed cathode sputtering systems [6,7] have been used for many years now to coat a variety of parts such as cutting tools or decorative pieces, and more recently three and four cathode systems [8,9] have been introduced. Parts being coated in a multi-cathode system will be coated from more than one side at a time, and there will be little or no shadowing. In a two cathode opposed system, there will be some side coating, but the part will never go into a shadow region. Three or four cathode systems eliminate this problem.

At the start of this program, BIRL was just bringing on line its unique opposed cathode sputtering system, which features a pair of opposed vertical magnetron sputtering cathodes with a target separation distance of either 15 or 28 cm. A schematic drawing of this coating system is shown in Figure 1. Three dimensional objects up to 15 cm in diameter by 30 cm long can be coated in this system, and the substrate table, which rotates, is located equidistant between the two cathodes. The stainless steel chamber, which is approximately 66 cm in diameter by 70 cm high, is surrounded with a water jacket, and either hot or cold water can be used for heating or cooling it. The sputtering chamber is double pumped. A 15 cm diffusion pump and a liquid nitrogen cold trap backed with a 80 cfm mechanical pump comprises the first pumping system whereas a 1500 l sec^{-1} turbomolecular pump backed with a combined 40 cfm roots blower and 40 cfm mechanical pump make up the second system. Two 20 kW dc power supplies provide power to the 12.7 cm by 38.1 cm sputtering targets, and a smaller 5 kW dc power supply is used for etching and substrate bias. Reactive gas partial pressure control is achieved with either a mass spectrometer feedback control system or with an Inficon OGC 1 system as has been described for our other reactive sputtering system [10,11].

Sputtering, until recently, had been limited in the amount of ion bombardment of the substrate that can be achieved during deposition of the coating. With conventional balanced magnetron (CBM) sputtering, there is a very high plasma

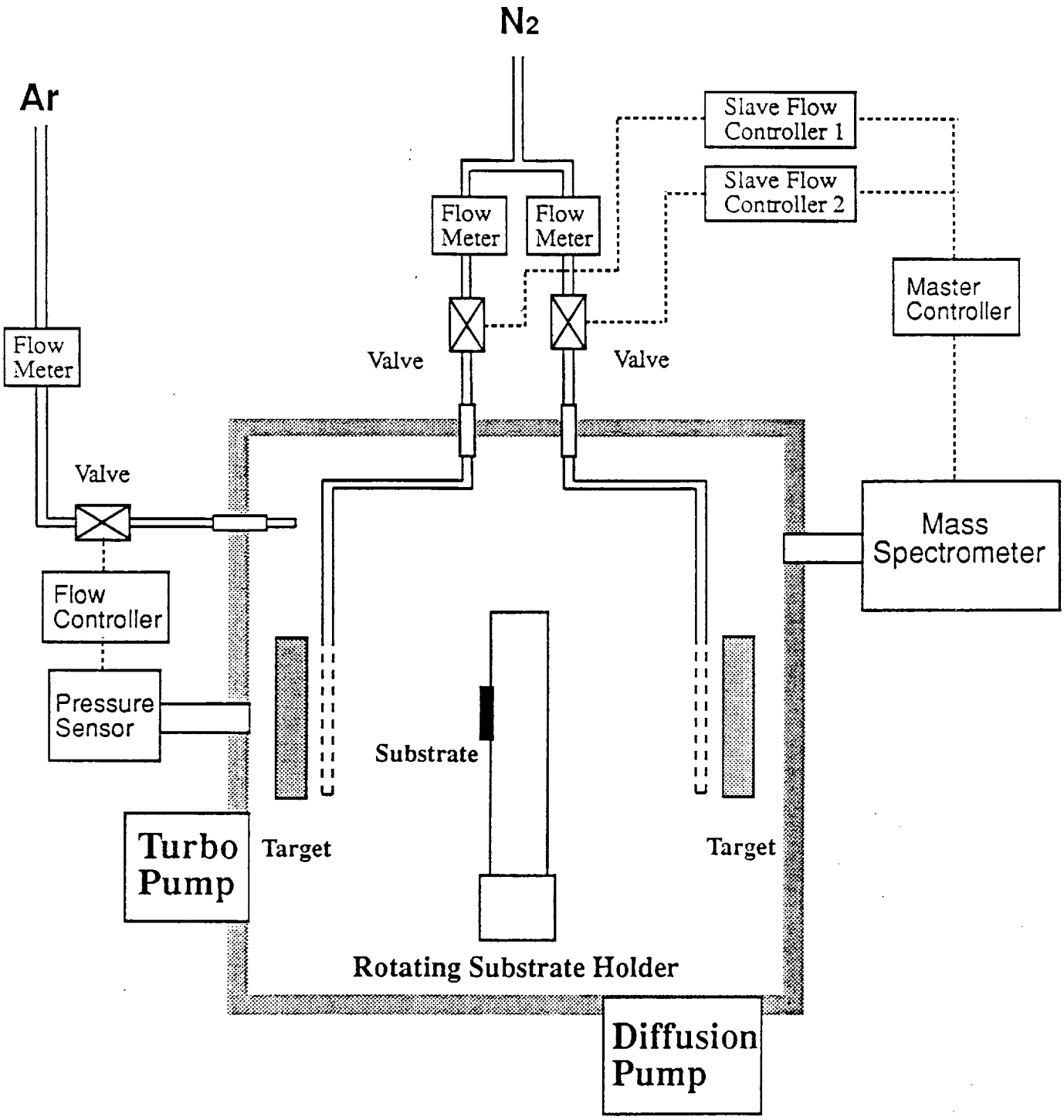

Figure 1. Schematic drawing of the opposed cathode unbalanced magnetron sputtering system.

density close to the sputtering target, but few of these ions reach out to the substrate region. When a negative bias potential is placed on the substrate during the growth of the film with CBM sputtering, the amount of current collected on the substrate, which is a measure of the amount of ion bombardment, will be relatively low. The substrate bias current quickly saturates as the bias potential is increased negatively because beyond a certain bias potential, which varies with target power and sputtering pressure, no more ions are available to be collected.

When the opposed cathode system (OCS) was initially tested, it was configured with two balanced magnetron sputtering cathodes equipped with AlNiCo magnets, and the substrate bias current density was very low, on the order of 0.4 mA cm^{-2}. This low substrate ion current density affected both the density and adhesion of the coating. Without adequate ion bombardment, the coatings produced in the opposed cathode system were porous along the grain boundaries, and the adhesion was low. It was necessary to correct this problem.

The substrate bias ion current density can be increased in a CBM sputtering system if the substrate is moved closer to the target, but there are limitations on how close the substrate can be placed near the target particularly if heat sensitive substrates are being coated. For large scale coating systems, reducing the distance is not practical. Triode sputtering systems where electrons are injected into the plasma either from a hot filament source or a hot hollow cathode [12] have been used in some instances to increase the substrate ion current density, but a triode system is much more complex to operate. Contamination from the wall material is a common problem in a triode systems. It was not until the introduction of unbalanced magnetron (UBM) sputtering by Window and Savvides [13-15] in 1986 that it was possible in a practical way to substantially increase the substrate bias ion current density during magnetron sputtering.

Unbalanced Magnetron Cathodes

A schematic drawing of a CBM sputtering cathode is shown in Figure 2 (a). In an idealized situation, most of the magnetic field lines loop between the inner and outer magnets, and the return field lines are contained by the steel

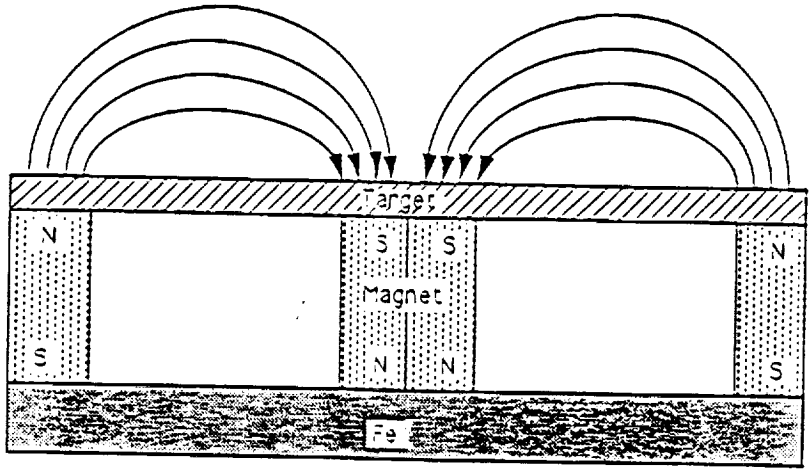

(a)

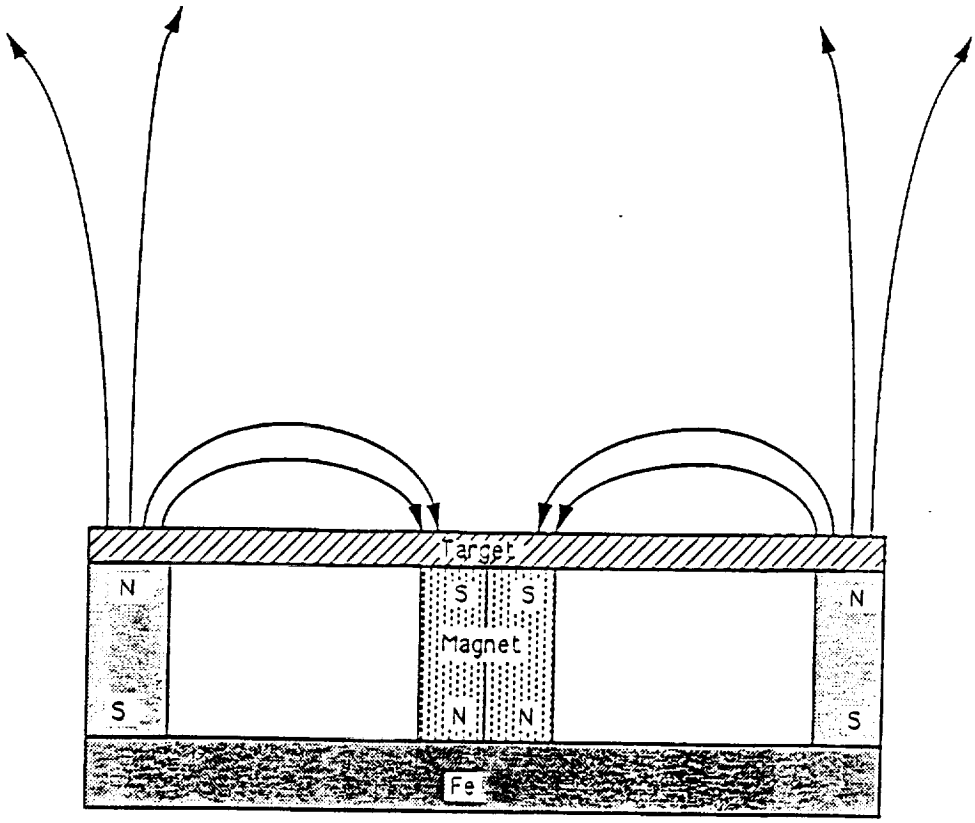

(b)

Figure 2. Schematic drawing of the balanced and unbalanced magnetron sputtering cathodes. (a) Balanced magnetron. (b) Window-Savvides type II unbalanced magnetron.

yoke to which the magnets are mounted. When the CBM is unbalanced, the strength of one set of the magnets, either the outer ones or the inner ones, is increased [15], which allows some of the magnetic field lines to expand away from the target surface as is shown in Figure 2 (b). For most work published to date, the cathode has been unbalanced by increasing the strength of the outer magnets, which is the Window and Savvides Type II UBM [13], but conceivably there are cases where one may want to reverse this orientation.

A CBM can be unbalanced with either permanent magnets or electromagnets. Electromagnets have the advantage that the strength of the magnetic field can be varied by changing the current flowing through the coil, and the degree of unbalance can be altered continuously within the current carrying capacity of the coil. Magnetic field strengths in an electromagnet are limited by the number of turns in the coil and by the amount of current that can flow through the coil before overheating becomes a problem. In addition, electromagnets are bulky, and their size can present design problems.

Permanent magnets, on the other hand, have fixed magnetic field strengths, and the composition (i.e., AlNiCo, NdFeB, etc.) and size of the permanent magnet determine the degree of unbalance in the cathode. Once the permanent magnet configuration is set in place, there is no variation in the magnetic field strength unless the magnets lose strength due to overheating or other causes. Permanent magnets normally require no cooling, but they must not become too hot. For the newer rare earth magnets, the field strengths are much higher than can be obtained practically from electromagnets.

In an UBM cathode, fast secondary electrons that escape from the cathode follow the magnetic field lines away from the target and undergo ionizing collisions with gas atoms. The plasma is not confined to the target area, and it expands away from the target surface. The density of this plasma depends on the number of ions formed, which in turn depends on how well the escaping electrons are confined by the magnetic field.

If the substrate is placed in this secondary plasma that forms away from the cathode surface, ions from the plasma are attracted to the substrate when a

bias is placed on the substrate. The number of ions that bombard the substrate depends on the density of the plasma at the substrate and the bias voltage. For a high current density to be collected at the substrate, the plasma density must be high in that area. The ions that are attracted to the substrate by the bias are those that have migrated to the substrate sheath region and have been accelerated across it by the bias voltage. Ions inside the plasma are protected by the plasma potential, and they do not feel the substrate potential unless they diffuse to the sheath region.

High current densities can be collected on the substrates in a UBM system. Window and Savvides [13] reported current densities as high as 9 mA cm^{-2} for a UBM cathode with permanent magnets. Musil and Kadlec [16], using a UBM system with electromagnets, have reported substrate bias current densities as high as 6 mA cm^{-2} at a target-to-substrate distance of 200 cm. These current densities equal or exceed those found in other successful PVD coating systems today.

Ion bombardment results in energy being put into a growing film, and the energy of the bombarding species is determined by the difference between the substrate bias potential and the plasma potential. In single cathode UBM systems, the plasma potential is usually at or near the anode potential, but in multi-cathode systems, the plasma potential can be negative with respect to the anode by as much as 20 volts [17]. The energy of the arriving ion species, then, is the difference between the bias and plasma potentials. Although the bias and plasma potentials determine the energy of the ion, the big difference between a CBM and UBM system is the number of ions bombarding the surface of the growing film. The ion current density usually is an order of magnitude higher or more in an UBM system compared to a CBM one.

Freller [18] reported that for the reactive sputtering of titanium nitride (TiN) the ion current density should be greater than 2 mA cm^{-2} in order to obtain a fully dense film. This number has received some attention lately, but what is really important is not just the substrate ion current density but the ratio of the number of bombarding ions to the number of arriving neutral atoms. Each bombarding ion will put a certain amount of energy into the

growing film, and the total number of ions arriving compared to the total number of neutral atoms is what influences the final properties of the film.

Ion to neutral ratios greater than one are usually desirable to achieve fully dense films. When the deposition rate is low, the neutral flux is low, and the substrate ion current density can also be low. When the deposition rate is increased, the ion current density must increase as well to maintain the ion to neutral ration. Fortunately, the substrate ion current density is proportional to the target power [19]. As the target power increases, the substrate ion current density also increases as does the deposition rate. The ion to neutral ratio depends greatly, then, on the design and operation of the UBM cathode or on its degree of unbalance.

Multi-Cathode Unbalanced Magnetron Systems

It was quickly recognized that multi-cathode UBM systems would be important for industrial applications of the UBM technology. Teer [8,20] reported on multi-cathode systems with three and four cathodes, and his company, Teer Coating Services in England, is now producing small and intermediate sized multi-cathode UBM systems. Münz [9,21] has also been very instrumental in the development of multi-cathode UBM systems, and his work has led to the introduction of a large scale four cathode system that combines the best features of both unbalanced magnetron sputtering and cathodic arc deposition. In this Arc-Bond Sputtering (ABS™) system that is now available from the Hauzer Techno Coating Company BV, which is located in Venlo, The Netherlands, the cathodic arc part of the process is used for the sputter etching of the samples, and the UBM part is used for the deposition of macroparticle free coatings.

This rapid introduction of UBM sputtering into the industrial arena is an indication of the importance placed on this new technology. All of the large scale multi-cathode UBM systems have evolved in order to be able to coat 3 dimensional parts. They all incorporate sputtering from multiple cathodes and substrate motion in order to overcome the substrate shadowing problem that is common with single cathode systems.

At BIRL, there are currently two large scale UBM systems in operation. The first BIRL system is the opposed, two-cathode UBM system, and the second is the Hauzer Techno Coating ABS™ system with four cathodes. As a result of BIRL's early involvement with the UBM technology for this NASA MSFC coating program, BIRL is the U.S. leader in this area.

The BIRL opposed cathode system was originally designed and built with two conventional balanced magnetron cathodes, but the substrate ion current density was very low. Most of the plasma in the system was confined next to each target, and there was very little plasma at the substrate. To overcome this problem, the cathodes were converted to Window-Savvides Type II unbalanced magnetron cathodes, and several different magnet configurations were evaluated [17,19,23-26] to determine the best combination to increase the substrate ion current density. After converting to a strongly unbalanced magnetron configuration with NdFeB magnets in the outer pole positions and AlNiCo magnets in the inner pole positions, the substrate ion current density was typically 5 to 6 mA cm^{-2} for a target power of 5 kW per target.

The success of the BIRL opposed cathode system today depends not only on unbalancing of the magnetrons, but it also depends on the orientation of the magnets in one cathode with respect to the ones in the other cathode. When the magnets in each cathode were arranged such that like poles faced like poles in the mirrored configuration [18] as is shown in Figure 3 (a), the current density was low. Interaction of the magnetic field lines from each cathode cause the field lines to bend toward the wall of the chamber, and fast secondary electrons are guided to the walls of the chamber. Few collisions occur between electrons and gas atoms in the vicinity of the substrate, and the plasma density is low there.

On the other hand, when the poles of the magnets are arranged such that opposite poles face each other as is shown in Figure 3 (b) in the closed-field opposed configuration, the vertical components of the magnetic fields from each set of magnets link up, and the magnetic field lines form a closed trap for the electrons. Escaping fast secondary electrons are guided into the region near the substrate where they undergo ionizing collisions with the

a.

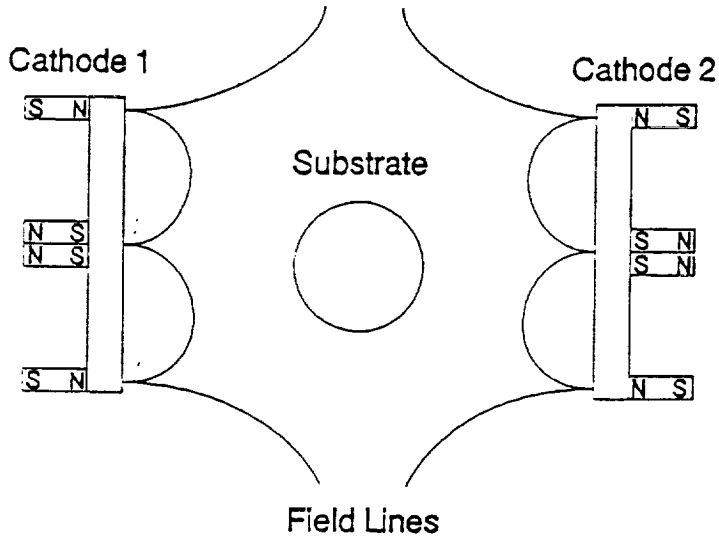

b.

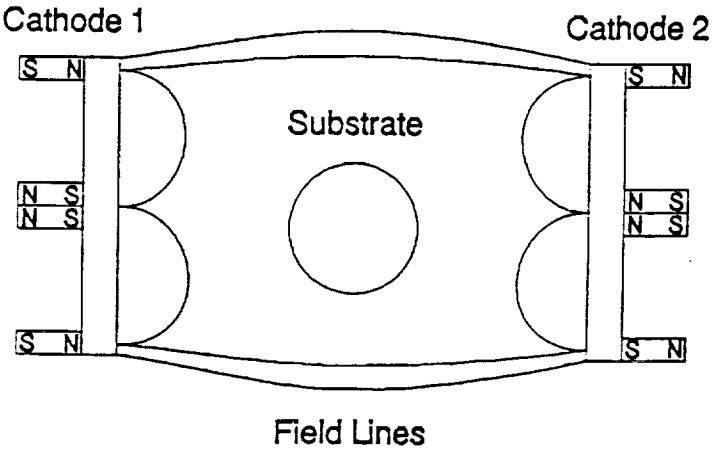

Figure 3. Mirrored and closed-field magnet configurations. (a) Mirrored. (b) Closed-field.

argon gas atoms. A relatively dense plasma forms near the substrate, and the amount of ion current collected on the substrate, depending on the degree of unbalance, can be quite high.
This linking of the magnetic fields is very important for multi-cathode systems, and it can only be achieved when there are an even number of cathodes. Whenever an odd number of cathodes is used, there will always be one pair of cathodes where linking cannot be achieved, and there will always be at least one escape path for the secondary electrons.

Results from six different magnet configurations for the BIRL opposed cathode system [22] are shown in Figure 4 in which the total current collected on the substrate as a function of sputtering pressure is shown. The six different magnet configurations are given in Table 1. The substrate used in this work

Table 1.
Six Magnet Configurations Used in UBM Study

Magnets				Magnetic field strength at chamber center-line, G
Set	Outer	Inner	Configuration	
A	AlNiCo	AlNiCo	Mirrored	0
B	AlNiCo	AlNiCo	Closed-field	<1
C	Double AlNiCo	AlNiCo	Mirrored	0
D	Double AlNiCo	AlNiCo	Closed-field	3
E	AlNiCo+NdFeB	Soft iron	Mirrored	0
F	AlNiCo+NdFeB	Soft iron	Closed-field	20

had a surface area of approximately 1000 cm^2, and thus the ordinate of the plot can read in mA cm^{-2} as well as amps. As the magnetron cathode becomes more and more unbalanced and when the magnetic fields are linked, two things happen. The current collected on the substrate increases, and the floating potential of the substrate increases negatively. With a strongly unbalanced magnetron cathode, as is shown for configuration F where the outer magnets are NdFeB+AlNiCo and the inner ones AlNiCo, current densities of 5 to 6 mA cm^{-2} are routinely collected on the substrate. This high current density contrasts

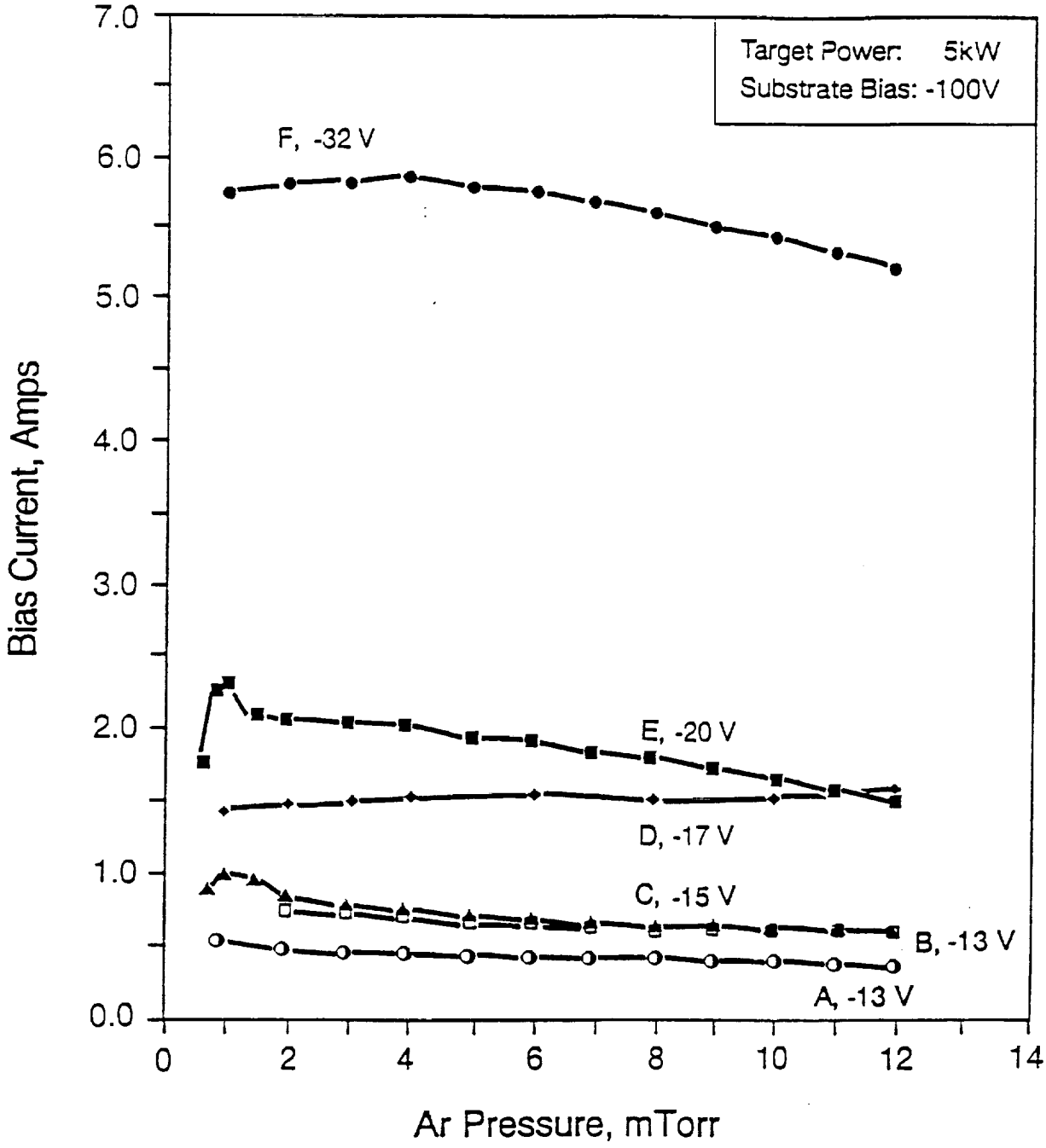

Figure 4. Substrate bias current as a function of sputtering pressure and cathode magnet configuration. See Table 1 for magnet configurations, A-F.

sharply with the low current density collected for the balanced, mirrored configuration as shown in curve A in Figure 4.

Magnetic fields play a very important role in the successful operation of UBM cathodes. Measurement of the magnetic fields with a hand-held Gauss meter in the BIRL opposed cathode system showed that the field strength in the vicinity of the substrate was only about 20 Gauss when configuration F was used (see Table 1). The substrate is held on a rotating table which is located equidistant between the two vertical cathodes that are separated by a distance of 280 mm. Other configurations produced an even smaller field strength at the substrate.

The hand measurement of the magnetic field strength was informative, but it was not until magnetic field modeling was done using finite element analysis for the different UBM systems that a good understanding of magnetic fields was achieved. This finite element analysis work [23,24] has shown for a single UBM cathode that as the strength of the outer magnets is increased, the strength of the parallel component (with respect to the surface of the target) increases. Typically for a balanced magnetron cathode that uses AlNiCo 5 magnets both on the inside and outside, the parallel component of the magnetic field has a strength of about 300 Gauss; but if NdFeB magnets are used on the outside and AlNiCo on the inside, the parallel component strength is about 500 Gauss.

When two UBM cathodes are arranged in an opposed configuration, the model shows that there is a great deal of interaction between the magnetic fields. When the cathodes are arranged in a mirrored configuration, components of the magnetic fields from each cathode repel each other, and the field lines are pinched together as they bend toward the chamber wall. Electrons follow these magnetic field lines toward the chamber wall, and there is a dense plasma at the pinch points, which are located opposite where the deposition rate is at its lowest point.

For the closed-field configuration, the model shows that the vertical magnetic field components from each cathode link up. The magnetic fields from the

outer magnets link up in one direction, while the magnetic fields from the inner magnets link up in the other direction. This linking forms a good magnetic trap for the electrons, and it is what makes the closed-field configuration so effective in increasing the substrate ion current density. The strength of the magnetic fields is predicted very well by the finite element analysis, and there is excellent agreement between the value predicted by the model and what is actually measured [19].

For a substrate rotating between the two cathodes in the BIRL opposed cathode system, the substrate ion current density, as measured with a Langmuir probe, is not constant [19], and it depends on the position of the substrate with respect to the targets as is shown in Figure 5. Both the mirrored and closed-field configurations show variations in the substrate bias current density as the substrate rotates through one revolution, but in all cases the substrate ion current density is highest for the closed-field configuration.

The position of the variation in substrate ion current density is important. For the mirrored configuration, the ion current density is highest where the neutral sputtered flux is lowest, whereas for the closed-field configuration, the ion current density is highest where the neutral flux is highest. The arrival rate of ions is basically in phase with the arrival rate of neutrals for the closed-field configuration, but it is out of phase for the mirrored configuration.

The dips in the substrate ion current density that are approximately 45° each side of the peak ion current shown in Figure 5 for the closed-field configuration are due to changes in sign of the magnetic field vector. The magnetic field modeling has shown that as the substrate rotates through one revolution in the closed-field configuration, it will pass through sign changes for the vertical components of the magnetic field. Each time the substrate passes through one of these sign changes, there is a zero point in the field where electrons can escape. These escape points show up as a low in the ion current density collected on the substrate [19].

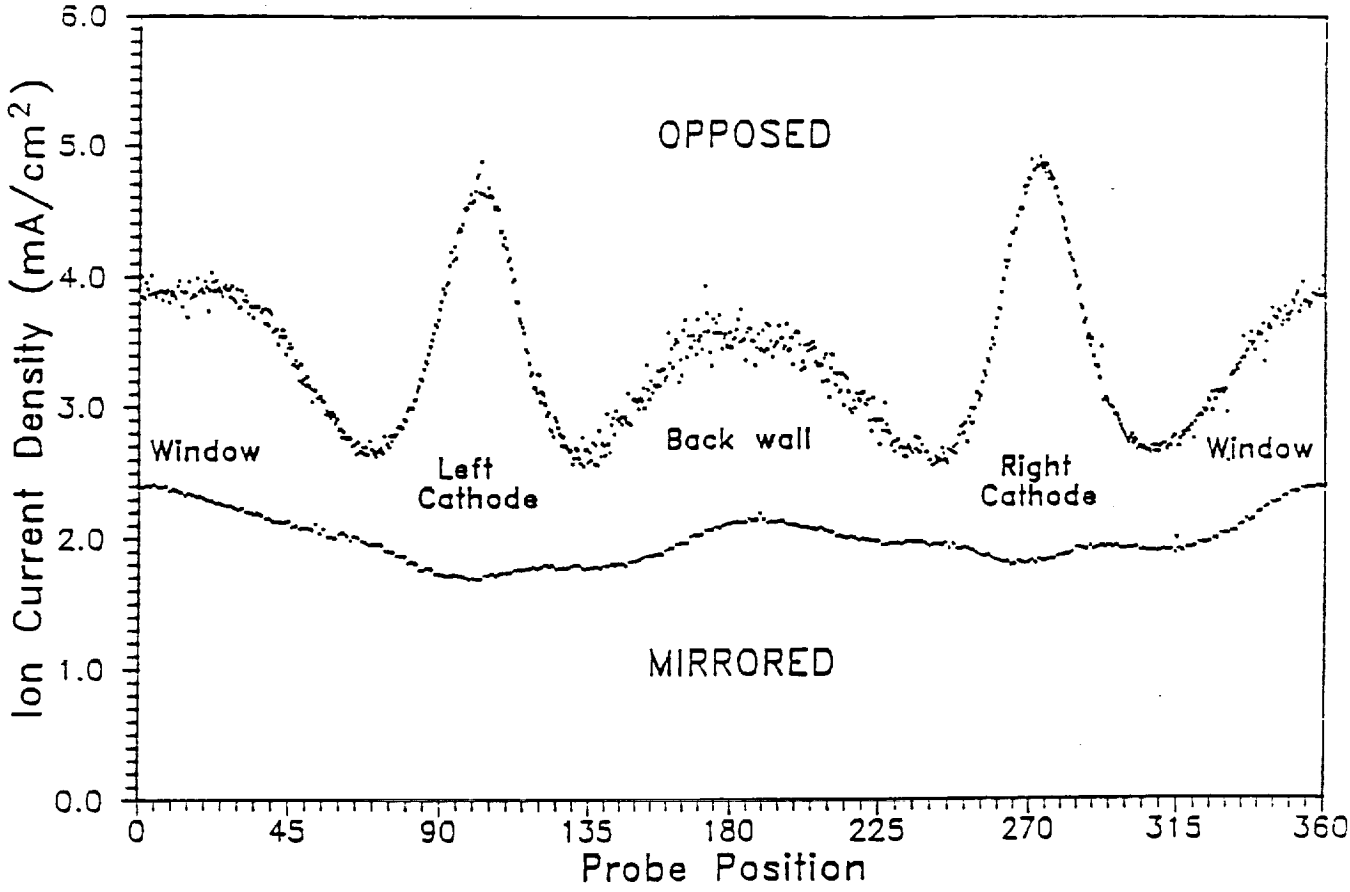

Figure 5. Substrate ion current density as a function of position around the substrate holder.

Recognizing the importance of UBM sputtering, BIRL sought additional sources of funding to promote the development of the UBM technology. Funding was obtained from the State of Illinois under their Department of Commerce and Community Affairs Challenge Grant Program to demonstrate that unbalanced magnetron sputtering is an industrial process. With this support and with funding from the U.S. Department of Energy, BIRL purchased and installed the four cathode Hauzer industrial scale unbalanced magnetron sputtering system, which made BIRL one of the leaders in the world with this technology. This large system, which has a chamber size of 1 m in diameter by 1 m high, incorporates one of BIRL's contributions to unbalanced magnetron sputtering - the linkage of the magnetic fields between the four cathodes. None of this growth in technology would have been possible without the original program from NASA MSFC. The expanded capabilities are now available to support advanced work on the development of industrial applications of the hard coatings.

The ion bombardment from UBM sputtering provides the energy to assure a fully dense, well adhered film, but there are cases where it can provide too much energy to the substrate. For example, when coatings are deposited on 440C stainless steel substrates, it is possible to overheat the substrate and soften the steel. It has been found that the amount of ion bombardment must be carefully controlled. The energy input must be high enough to achieve the desired properties in the film, but it must not be so high that it overheats the steel. It is definitely a delicate balancing act, one in which we are still learning the rules of the road.

It is not just the ion bombardment that contributes to the potential softening of the steel substrates, but there are many other sources of energy input to the substrate that contribute to its heating. Before any substrate is coated, it is given a final cleaning *in situ* with a sputter etch, which is another form of ion bombardment that contributes to the heating of the specimen. Once the sputter etch is completed, coating begins, and there are several sources of energy input during coating. Among these sources of energy input are the heat of condensation of the vapor flux, the heat of reaction from the formation of the compound, the radiant heating from the sputtering targets,

the hot gases in the plasma, and the ion bombardment. All of these sources of heating must be considered when trying to control the energy input into the growing film.

COATING DEPOSITION

By the end of the 1980's, it had been shown that titanium nitride (TiN) coatings could lead to significant improvements in the rolling contact fatigue (RCF) life of bearing elements and that there was a coating thickness dependence for this improvement [25-31]. The work by Cheng et al. [32] and by Chang et al. [33,34] expanded the earlier work on the RCF life of TiN coatings on bearing steels. As long as the coating was less than 1 μm thick, the TiN coating could increase the life of RCF elements.

Although the improvement in RCF life had been shown with TiN coatings, there was a need to demonstrate that TiN could be applied consistently to steel substrates without significantly changing the metallurgical properties of the substrate and that the technology could work on an industrial scale. In addition, all of the early work had been done with TiN, and it was not known if other hard coatings deposited by low temperature physical vapor deposition techniques would also lead to improvements in the RCF life of coated elements.

BIRL undertook the sputter coating program for the NASA MSFC to demonstrate that unbalanced magnetron reactive sputtering could be used to deposit eight different nitride coatings and two pure metal coatings onto 440C stainless steel without significantly changing the metallurgical properties of the steel. The coatings were deposited onto RCF test rods, and the coated specimens were sent to NASA MSFC for RCF testing. The eight coatings that were evaluated were titanium nitride (TiN), zirconium nitride (ZrN), hafnium nitride (HfN), chromium nitride (CrN), ß-molybdenum nitride (ß-Mo_2N), titanium-aluminum nitride ($Ti_{0.5}Al_{0.5}N$), titanium-zirconium nitride ($Ti_{0.5}Zr_{0.5}N$), and titanium-aluminum-vanadium nitride (Ti-Al-V)N, and the two pure metal coatings were gold (Au) and copper (Cu).

Coating Experimental Procedures

All of the reactive nitride coating work was done in the BIRL opposed-cathode, unbalanced-magnetron sputtering system, and details of this system were given above. The Cu and Au coatings were deposited in the single cathode balanced magnetron 902M Materials Research Corporation (MRC) in-line sputtering system. High purity argon (99.999%) was used as the sputtering gas, and high purity nitrogen (99.9995%) was the reactive gas for all nitride coatings. Automatic feedback control was used to maintain the partial pressure of the reactive gas at the desired set point during the deposition of the nitride coatings, and two different control systems were used over the course of this program. Either an Inficon OGC by itself or an Inficon Quadrex 100 quadrupole mass spectrometer in conjunction with MKS mass-flow controllers was the instrument used to achieve automatic feedback control of the reactive gas [35].

A pair of opposed, vertically mounted MRC Mu Inset™ sputtering cathodes, modified with NdFeB magnets to make them strongly unbalanced, were used in the opposed-cathode system for the deposition of the nitride coatings. Target power (dc) to each cathode was usually 5 kW. A dc substrate bias was used during the deposition of all coatings, and the substrate bias could be varied between the floating potential (on the order of -30 V) up to a maximum of -1000 V. Typically the bias voltage was in the -50 to -100 V range. For the deposition of the metal coatings, a single MRC Mu Inset™ balanced magnetron sputtering cathode was used. For the deposition of the gold, the target power was 0.5 kW, and for the copper, the target power was 1.0 kW. Low target powers were used with the metals because they both sputter at very high rates.

All of the sputtering targets were the MRC Mu Inset™ shaped targets, and the target materials were either MRC VP or Marz grade. The ten target materials were Ti, Zr, Hf, Mo, Cr, Cu, Au, 50-50 at.% Ti-Al, 50-50 at.% Ti-Zr, and Ti-Al-V, which is the aircraft titanium alloy with a composition of 6 wt.% Al, 4 wt.% V, and the remainder Ti.

Two different types of substrates were used in this program. Rectangular test blocks (1.2 x 2.5 x 0.6 cm) of two different steels were used as substrates in the development of each coating; and then once the parameters for depositing

the desired coating had been established, cylindrical RCF rods were used. The rectangular blocks were either pieces of hardened M2 high speed tool steel (60 Rc) or 440C stainless steel (60 Rc). The RCF substrates, which were all from the same fabrication batch, were hardened 440C stainless steel (nominally 59 Rc) rods with a diameter of 9.5 mm and a length of 75 mm. Prior to being placed in the sputtering chamber, all of the substrates were ultrasonically cleaned with acetone and then alcohol.

In the opposed-cathode sputtering chamber, the rectangular substrates were mounted at the midpoint of a long cylindrical substrate holder (7.5 cm dia. by 38 cm), which typically rotated at a speed of 10 rpm during deposition. The RCF rods were mounted in a planetary fixture that provided two-fold rotary motion to assure uniform coverage of the samples. Up to six substrates could be held in the planetary fixture, and the height of this fixture was set such that the RCF rods were opposite the middle of the cathodes. Rotation speed of the planetary fixture was again typically 10 rpm; and for each turn of the fixture, each rod turned 1.33 times. In the single-cathode chamber, the rectangular blocks were placed in the center of a 31 cm x 31 cm square pallet, and the rods were mounted in a self contained rotary fixture pallet.

Once the opposed-cathode chamber was pumped down to a base pressure of at least 2×10^{-6} Torr, it was back filled with argon to a working pressure of 30 mTorr, and the samples were given a dc sputter etch for 15 minutes with a substrate bias of -700 V. After the etch, the argon pressure was reduced to the range of 6 to 8 mTorr, the reactive gas was turned on, power was applied to the targets and the substrate, and the reactive deposition was begun for the nitride coatings. Target power, substrate bias voltage, reactive gas partial pressure (when used), and total pressure were maintained constant throughout the deposition run.

The coating sequence was similar in the single cathode system. Once the chamber had reached a base pressure of 2×10^{-7} Torr, the chamber was back filled with argon to a pressure of 2 mTorr, and the samples were given a 1.5 Kw rf etch for 5 minutes. Once the etch was completed, the samples were moved from the etch station to a position under the target. No scanning motion was

used while the samples were coated, but the RCF rods were rotated while the samples were being coated. No reactive gas was used during the deposition of the Cu and Au coatings.

Coating thickness was controlled by the length of time of the deposition, and four different coating thicknesses, 0.25, 0.50, 0.75, and 1.0 μm, for each type of coating were sputtered onto the RCF test rods. For hardness and adhesion tests, thicker coatings in the range of 3 to 5 μm were deposited onto the rectangular test blocks.

The nitride coatings were characterized for hardness, adhesion, and crystal structure. The hardness of the coatings was measured with a Leco DM-400FT microhardness tester, which has flat field optics and magnification up to 1000X, and all microhardness values reported in this paper were taken with a 25 gf load. The adhesion of the coatings was measured with the manual CSEM Revetest, and a Scintag X-ray diffraction unit using CuKα radiation was used to determine the crystal structure of the coatings. The hardness of the 440C stainless steel RCF test rods was measured before and after coating with a Rockwell C indentor, and the measurements were made on the side of the rods before and after coating at a distance of 0.5 cm from each end and in the middle of the each rod.

Coating Results

Throughout the deposition phase of this program, the goal was to produce a hard (for the nitride coatings), well-adhered coating on the 440C stainless RCF test rods without significantly changing the metallurgical properties of the steel. Three of the coatings, TiN, ZrN, and HfN, had been reactively sputtered in previous work [36], but experience was lacking for the other seven coatings that were to be produced in this program. For each coating, a range of deposition conditions were explored, and the deposition conditions chosen for the nitride coating of the RCF rods were those that produced the best combination of hardness and adhesion. Since the Au and Cu coatings are soft and were to be used as a "quasi-lubricant," coating hardness was not a criteria for these two materials. The deposition conditions along with the

resulting deposition rate, hardness, and adhesion are given in Table 2 for each of the ten coatings.

Only two of the four deposition parameters, substrate bias voltage and nitrogen partial pressure, varied much from run to run for the nitride coatings. The biggest changes in the nitrogen partial pressure were for CrN and ß-Mo_2N. All of the titanium based coatings plus ZrN and HfN required a nitrogen partial pressure in the range of 0.1 to 0.21 mTorr, whereas CrN and ß-Mo_2N needed partial pressures of 2.1 and 1.0 mTorr, respectively, to produce the stoichiometric compositions due to the lower affinities of these metals for nitrogen. Bias voltage varied from -50 to -100 V, but even at the lower bias voltage of -50 V, the hardnesses of ZrN and HfN were equivalent to values found in previous work [36]. Total system pressure was varied only a small amount, from 6 to 8 mTorr for the nitride coatings and 2 to 8 mTorr for the metal coatings, and these pressures were used because they produced good properties in the coatings.

The target power was the same for seven of the eight nitride coatings, but it was reduced for $Ti_{0.5}Al_{0.5}N$ because the 440C stainless steel RCF rods were overheating and softening during deposition. The high ion flux available at the substrate in this opposed-cathode, unbalanced-magnetron sputtering system can be both helpful and harmful. The high ion flux can assure a fully dense, well adhered coating; but it can also overheat the substrate, particularly for materials like 440C stainless steel, which begins to soften at 250°C. By lowering the target power to 3 kW per target during the deposition of $Ti_{0.5}Al_{0.5}N$, it was possible to minimize the softening of the steel. Substrate overheating was not a problem with the metal coatings because the high sputter yields for these two materials allowed them to be deposited quickly at low target powers.

Another way to avoid the overheating problem is to add heat sinks to the substrates during deposition of the coatings. The RCF rods initially were held only at the bottom of the sample during coating; but when a cylindrical heat sink was added to the top of the specimen, the overall temperature of the specimen was reduced during coating. Although heat sinks were not used with

Table 2.
The Deposition Conditions, Growth Rate, Hardness, and Scratch Adhesion Test Critical Load (and the thickness for the test) for the Ten Coatings.

Coating Material	Deposition Conditions				Coating		
	Target Power, kW per target	Pressure, mTorr		Negative Substrate Bias, V	Deposition Rate, $\mu m\ hr^{-1}$	Hardness (25 gf), $kgf\ mm^{-2}$	Critical Load (Thickness), kgf (μm)
		Total	N_2 Partial				
TiN	5	6	0.21	75	4.5	2200	5.5 (4.0)
$Ti_{0.5}Al_{0.5}N$	3	8	0.21	80	5.1	1900	4.5 (4.6)
$Ti_{0.5}Zr_{0.5}N$	5	8	0.12	70	6.9	2800	4.5 (4.6)
(Ti-Al-V)N	5	6	0.20	100	4.2	2200	4.0 (4.0)
ZrN	5	6	0.10	50	7.4	2600	5.5 (3.7)
HfN	5	6	0.15	50	7.2	2600	4.0 (3.6)
CrN	5	8	2.1	75	6.0	1900	6.0 (3.0)
β-Mo_2N	5	8	1.0	100	10.0	2300	5.0 (5.0)
Au	0.5	2	-	50	5.3	-	-
Cu	1.0	8	-	100	4.5	-	-

the CrN and $Ti_{0.5}Al_{0.5}N$ samples, they were used with most of the other coatings, and they were effective in minimizing the reduction in hardness of the 440C stainless steel substrates.

All of the nitride coatings gave good scratch-adhesion-test critical loads on the test blocks, and the assumption was made that the deposition conditions that produced these good critical loads would also work when thinner coatings were deposited on the RCF test rods. The hardnesses of the nitride coatings are all excellent with one exception. In hindsight, the hardness for the $Ti_{0.5}Al_{0.5}N$ coating is probably lower than it should be [37,38]. This $Ti_{0.5}Al_{0.5}N$ coating did not perform well in the RCF tests, and the poor performance may have been due to the low hardness of the coating. Except for CrN and $Ti_{0.5}Al_{0.5}N$, all of the other nitride coatings led to significant improvements of the Weibayes B10 life for the coated RCF test rods as will be shown shortly. The hardness of (Ti-Al-V)N, 2200 kgf mm^{-2}, is also slightly lower than the values of 2500 to 3000 kgf mm^{-2} reported by Knotek et al. [39] and is within the range of 2100 to 3600 kgf mm^{-2} reported by Münz [40].

The deposition rates for these eight nitride coatings varied by more than a factor of 2. The highest deposition rate was for ß-Mo_2N at 10 $\mu m\ hr^{-1}$, and the lowest was 4.2 $\mu m\ hr^{-1}$ for (Ti-Al-V)N. The ß-Mo_2N coating performed very well in the RCF tests, and this performance combined with its high deposition rate make it a leading candidate as a protective coating for RCF elements.

One of the questions raised in this program concerned which phase of chromium nitride and molybdenum nitride to use. By increasing the nitrogen partial pressure and keeping the other deposition parameters constant, different phases of chromium and molybdenum nitride were formed. For CrN_x, the first phase to form was a solid solution of nitrogen in Cr, followed with increasing nitrogen by Cr_2N, and finally CrN [41]. Molybdenum was similar, but the sequence was a solid solution of nitrogen in Mo, the body-centered tetragonal ß-Mo_2N, and finally the face-centered cubic γ-Mo_2N [42]. Although there were indications from the X-Ray diffraction patterns that an MoN phase might be present, it was never conclusively shown that MoN had been made.

When it was time to make the RCF test samples for MoN_x and for CrN_x, it was necessary to choose from the phases that could be reactively sputtered in the opposed-cathode system. Since there were no reported data on the performance of any of these MoN_x or CrN_x phases in RCF situations, it was decided to pick ones that gave both high hardness and good adhesion. The ß-Mo_2N and CrN phases were chosen, and the former performed well in the RCF tests, whereas the latter did not. CrN may have done well if the substrate had not been softened, and additional tests are needed to determine if it was the substrate or the material that led to the early RCF failure with the CrN coatings.

The lattice parameters for all nitride eight coatings are given in Table 3, and these lattice parameters were calculated from the X-ray diffraction patterns shown in Figures 6 and 7. The lattice parameters for TiN, ZrN, HfN, and CrN, are all greater than the bulk values reported in the JCPDS Powder diffraction file [43], but they are similar to what has been reported in the literature [35,44] for these sputtered coatings. The expansion in these lattice parameters is probably due to high compressive residual stress in the films, but residual stress measurements have been made only on the TiN films at BIRL, which verified the high compressive residual stress. The lattice parameters for ß-Mo_2N are virtually the same as reported in the JCPDS Powder diffraction file [45], and they are the same as reported by Perry et al. [46] for reactive cathodic arc deposited ß-Mo_2N. The lattice parameter for $Ti_{0.5}Al_{0.5}N$ is smaller than the value of 4.18 Å that Håkansson et al. [37] or McIntyre et al. [38] reported for a $Ti_{0.5}Al_{0.5}N$ film grown with zero bias. The value of the lattice parameter for (Ti-Al-V)N, 4.258 Å, falls within the range of lattice parameters that Knotek et al. [39] reported for their material of similar composition. Knotek et al. [47] working with $Ti_{0.7}Zr_{0.3}N$ reported a lattice parameter of 4.36 Å for this material compared to the value of 4.394 Å for $Ti_{0.5}Zr_{0.5}N$ prepared in this program.

The orientation of the nitride coatings varied from material to material as is also shown in Table 3. TiN had strong (111), (200), and (220) peaks, whereas ZrN, $Ti_{0.5}Al_{0.5}N$, $Ti_{0.5}Zr_{0.5}N$, and (Ti-Al-V)N were all strongly oriented in the (111) direction. HfN and ß-Mo_2N were both strongly oriented in the (200) direction, while CrN was strongly (220).

Table 3.
X-Ray Diffraction Results for the Eight Nitride Coatings.

Coating Material	Structure	Lattice Parameter(s), Å	Relative Intensity of XRD Peaks					
			(111)	(200)	(220)	(311)	(222)	(400)
TiN	fcc	4.264	90	100	70	14	9	-
$Ti_{0.5}Al_{0.5}N$	fcc	4.165	100	2	<1	<1	<1	-
$Ti_{0.5}Zr_{0.5}N$	fcc	4.394	100	9	19	9	<1	-
(Ti-Al-V)N	fcc	4.258	100	7	14	<1	12	-
ZrN	fcc	4.604	100	4	2	<1	5	-
HfN	fcc	4.562	10	100	3	3	-	4
CrN	fcc	4.198	15	65	100	8	<1	-
β-Mo_2N	bc tetragonal	a = 4.212 c = 8.064	(112) 35	(200) 100	(004) 4	(220) 3	(204) 9	-

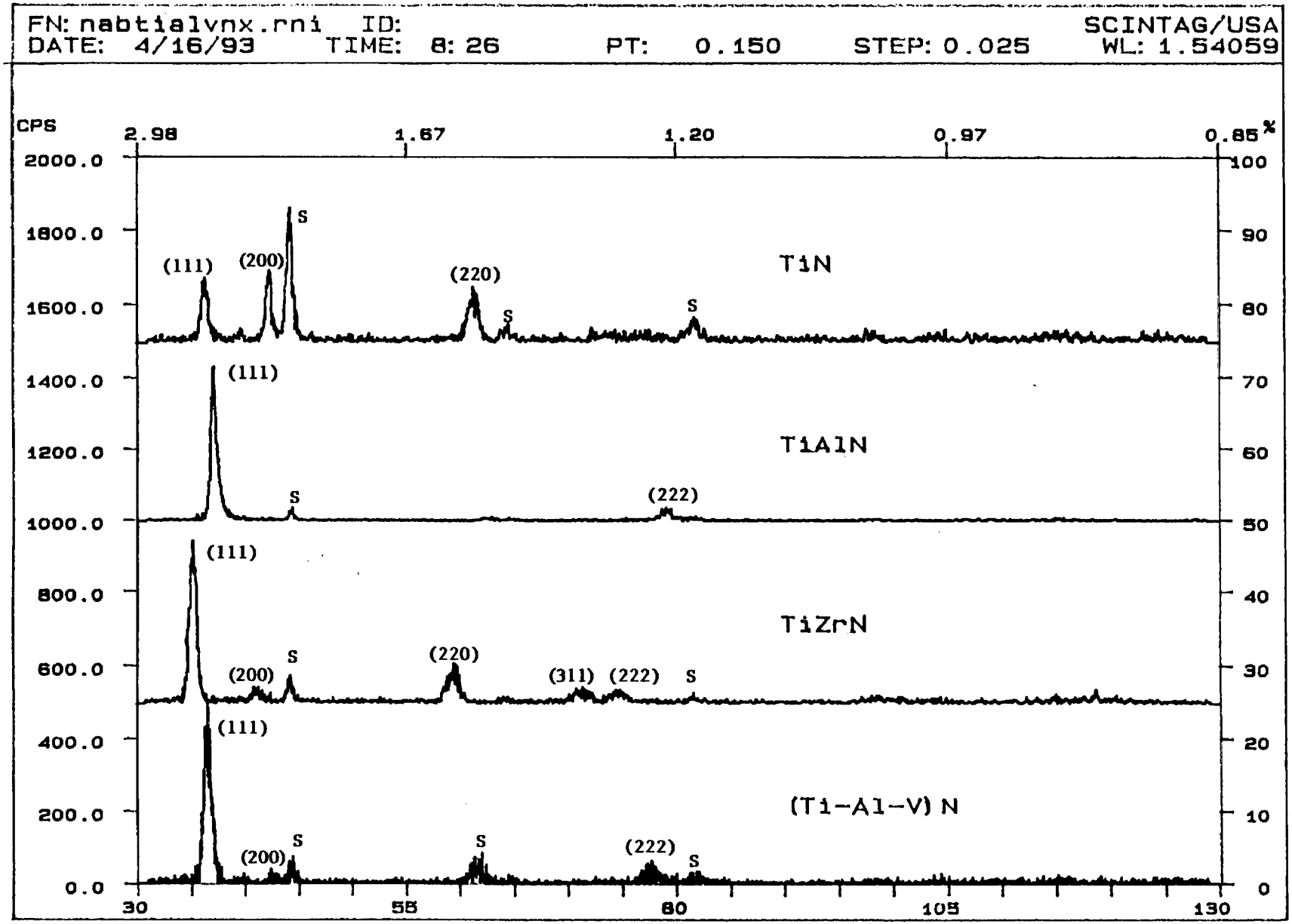

Figure 6. X-ray diffraction plots for the for titanium compounds.

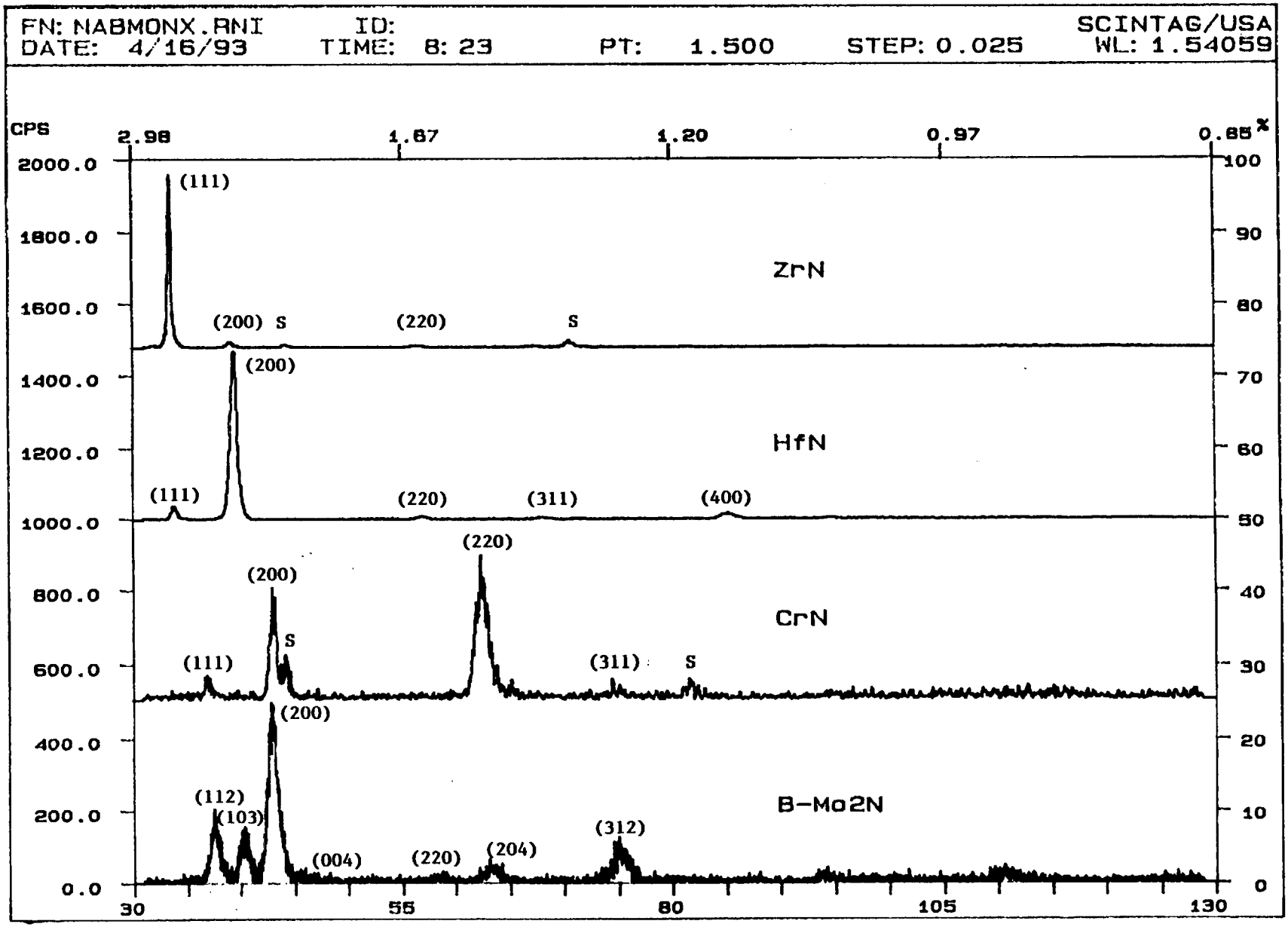

Figure 7. X-ray diffraction plots for the non-titanium compounds.

Coating Structure

The structure of the hard nitride coatings is columnar as is shown in Figure 8 for TiN on the steel substrate. The coating is very dense, and there is a thin titanium layer between the substrate and the TiN coating that helps to enhance the adhesion of the coating. The columnar structure of this coating is typical of reactively sputtered hard coatings.

ROLLING CONTACT FATIGUE TESTING

All of the RCF testing was carried out at MSFC under the direction of Robert Thom and Lewis Moore in the Tribology Research Branch (EH14). Even though the RCF tests were not done at BIRL, the results of these tests are included in this report for completeness. At the time of the writing of this report, all of the RCF tests had been completed for the eight nitride coatings, but they had not been completed for the two metal coatings. Final results for the nitride coatings but only preliminary results for the metal coatings will be given here.

RCF Test Procedures

The rolling contact fatigue tests were carried out on a three-ball-on-rod RCF tester, developed by Federal-Mogul [48] and now made by NTN. For the entire RCF test program, two different spring thrust loads were used to produce two Hertz stress conditions of 4.0 and 5.4 GPa, respectively. On each coated specimen (rod), seven individual RCF tests were conducted with a Hertz stress of 4.0 GPa and another seven RCF tests were under the Hertz stress of 5.4 GPa. The rotational speed of the test rods was 3600 rpm, corresponding to a surface speed of 1.8 m s^{-1}. A synthetic jet turbine engine lubricant, MIL-L-7808J lot 37, was supplied to the test specimen by a drip feed to maintain the lubricated condition. Eight RCF tests were run simultaneously with multiple ball-rod test machines. The individual RCF test was automatically terminated when vibration from a fatigue spall was detected by an accelerometer. The tests were timed in hours, and the time was converted to the number of cycles to fatigue failure by multiplying by a factor of 516,024 cycles per hour. The RCF lives of each coating material and thickness were analyzed using Weibayes statistics, which is essentially a Weibull analysis with an assumed slope of the distribution line. In each of these cases, a slope of 2 was used, which

Figure 8. Cross-section transmission electron micrograph of a TiN coating on steel.

has been found to be typical from similar RCF test experience at Marshall Space Flight Center [49]. For the nitride coating RCF tests, roughened loading balls with an Ra surface roughness of 0.089 μm obtained from NTN were used to cyclically stress the test specimens. These roughened balls provice a more severe test of the bearing material and any surface films than a ball with a relatively smooth surface. For the metal coatings, smooth balls with an Ra surface roughness of 0.013 μm were used to cyclically stress the test specimens. The roughness of these smooth balls would be more typical of balls used in actual bearings.

The hardness of the 440C stainless steel test rods was measured before and after coating with a Rockwell C indentor, which was calibrated with a test block of hardness Rc 63.9 to measure within ± 0.5 Rc of this value. Hardness measurements were made on the side of the rods before and after coating at a distance of 0.5 cm from each end and in the middle of each rod. These three values before and after coating were averaged, and any difference between the two averages was noted.

RCF Test Results

Nitride Coatings

Rolling contact fatigue test results of the nitride coated 440C stainless steel rods are given in Tables 4 and 5 in which the Weibayes B10 life for failure for each coating and thickness is given, both in hours and number of cycles, for each of the stress levels. In addition, the tables also show the improvement factor for the particular coating material and thickness compared to uncoated baseline test rods, which collectively (42 tests) had a Weibayes B10 life of 6.30×10^6 and 1.7×10^6 cycles for Hertzian stresses of 4.0 and 5.4 GPa, respectively. Finally, the average hardness of the test rod measured before and after coating along with the difference between these two averages is given in these tables.

The Weibayes B10 life for each coating, thickness, and stress level from Tables 4 and 5 is also plotted with bar charts in Figures 6-9. The bar charts are grouped by contact stress, 4.0 and 5.4 GPa, and for titanium and non-titanium nitride materials for each stress. The order of the coatings on the

Table 4.
Results of Rolling Contact Fatigue Tests for TiN, $(Ti_{0.5}Al_{0.5})N$, (Ti-Al-V)N, and $(Ti_{0.5}Zr_{0.5})N$ Coatings

Rod Number	Coating		Weibayes B10 Life				Improvement factor over baseline		Rod Hardness, Rc		
	Material	Thick-ness, μm	Hours		10^6 Cycles		4.0 GPa	5.4 Gpa	Before Coating	After Coating	Decrease
			4.0 Gpa	5.4 Gpa	4.0 GPa	5.4 GPa					
	Baseline	0	12.2	3.3	6.3	1.7	1.0	1.0	59.1	-	0
491	TiN	0.25	11.1	7.4	5.7	3.8	0.9	2.3	59.1	57.4	1.7
446		0.50	70.0	16.9	36.1	8.7	5.7	5.2	59.2	57.4	1.8
444		0.75	42.5	11.9	21.9	6.1	3.5	3.6	59.0	57.9	1.1
493		1.00	20.6	8.2	10.6	4.2	1.7	2.5	59.3	57.6	1.7
525	$(Ti_{0.5}Al_{0.5})N$	0.25	6.2	2.7	3.2	1.4	0.5	0.8	58.9	58.0	0.9
536		0.50	8.5	10.3	4.4	5.3	0.7	3.1	58.8	57.9	0.9
523		0.75	5.1	3.1	2.6	1.6	0.4	0.9	58.9	55.5	3.4
503		1.00	10.0	4.8	5.1	2.5	0.8	1.5	59.1	56.4	2.7
526	(Ti-Al-V)N	0.25	14.3	6.7	7.4	3.5	1.2	2.0	58.5	58.3	0.2
538		0.50	92.9	19.9	47.9	10.3	7.6	6.1	59.2	58.3	0.9
527		0.75	36.0	20.1	18.6	10.4	3.0	6.1	58.2	56.1	2.1
529		1.00	39.7	14.6	20.5	7.5	3.3	4.5	59.4	58.2	1.2
516	$(Ti_{0.5}Zr_{0.5})N$	0.25	7.8	12.5	4.0	6.4	0.6	3.8	59.3	59.0	0.3
515		0.50	41.7	20.9	21.5	10.8	3.4	6.4	59.4	58.8	0.6
514		0.75	22.3	10.1	11.5	5.2	1.8	3.1	59.0	58.3	0.7
513		1.00	37.8	10.4	19.5	5.4	3.1	3.2	59.8	58.1	1.7

Table 5.
Results of Rolling Contact Fatigue Tests for CrN, HfN, Mo_2N, and ZrN Coatings

Rod Number	Coating		Weibayes B10 Life				Improvement factor over baseline		Rod Hardness, Rc		
	Material	Thick-ness, μm	Hours		10^6 Cycles		4.0 GPa	5.4 GPa	Before Coating	After Coating	Decrease
			4.0 GPa	5.4 GPa	4.0 GPa	5.4 GPa					
	Baseline	0	12.2	3.3	6.3	1.7	1.0	1.0	59.1	-	0
495	CrN	0.25	6.2	1.0	3.2	0.5	0.5	0.3	59.1	55.5	3.6
497		0.50	5.0	1.9	2.6	1.0	0.4	0.6	58.7	56.0	2.7
501		0.75	41.8	3.9	21.6	2.0	3.4	1.2	58.8	55.6	3.2
502		1.00	4.3	1.7	2.2	0.9	0.4	0.5	59.2	56.1	3.1
448	HfN	0.25	39.2	6.8	20.2	3.5	3.2	2.1	59.1	58.7	0.4
445		0.50	156.9	38.3	81.0	19.7	12.9	11.7	59.2	58.6	0.6
539		0.75	25.4	9.5	13.1	4.9	2.1	2.9	59.1	58.5	0.6
500		1.00	67.9	9.6	35.0	5.0	5.6	2.9	58.9	58.0	0.9
531	Mo_2N	0.25	21.8	28.6	11.3	14.8	1.8	8.7	59.1	58.7	0.4
537		0.50	23.2	11.5	12.0	5.9	1.9	3.5	59.1	58.5	0.6
534		0.75	77.3	9.7	39.9	5.0	6.3	3.0	58.8	57.9	0.9
532		1.00	52.4	26.7	27.0	13.8	4.3	8.1	59.0	58.3	0.7
512	ZrN	0.25	4.4	1.9	2.3	1.0	0.4	0.6	58.4	59.0	-0.6
540		0.50	36.2	4.1	18.7	2.1	3.0	1.3	59.8	58.6	1.2
511		0.75	71.1	10.7	36.7	5.5	5.8	3.3	58.9	58.7	0.2
541		1.00	38.3	25.0	19.8	12.9	3.1	7.7	59.4	58.9	0.5

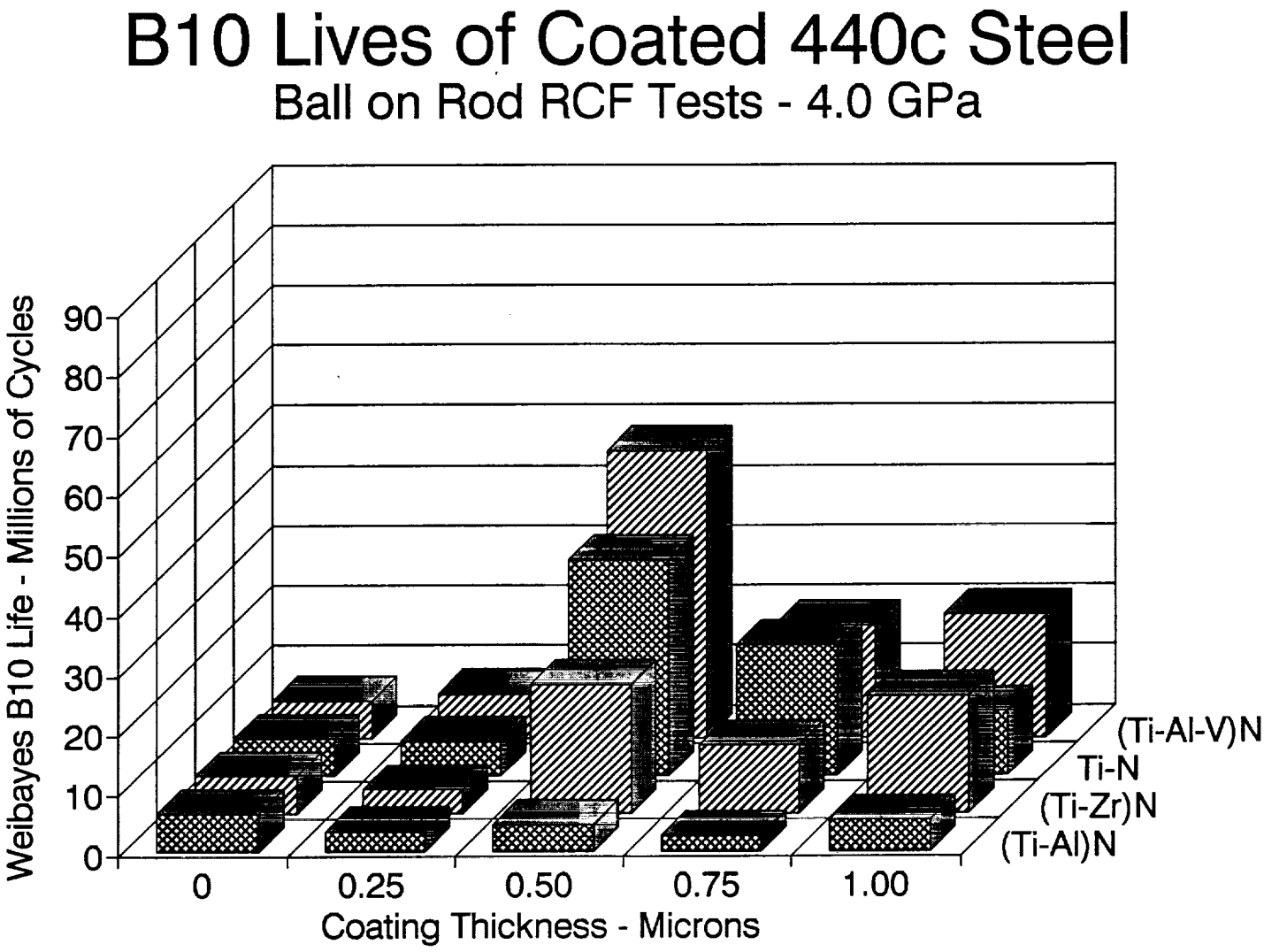

Figure 9. B10 lives of coated 440C stainless steel. Ball on rod RCF tests conducted at 4.0 GPa for the titanium compounds.

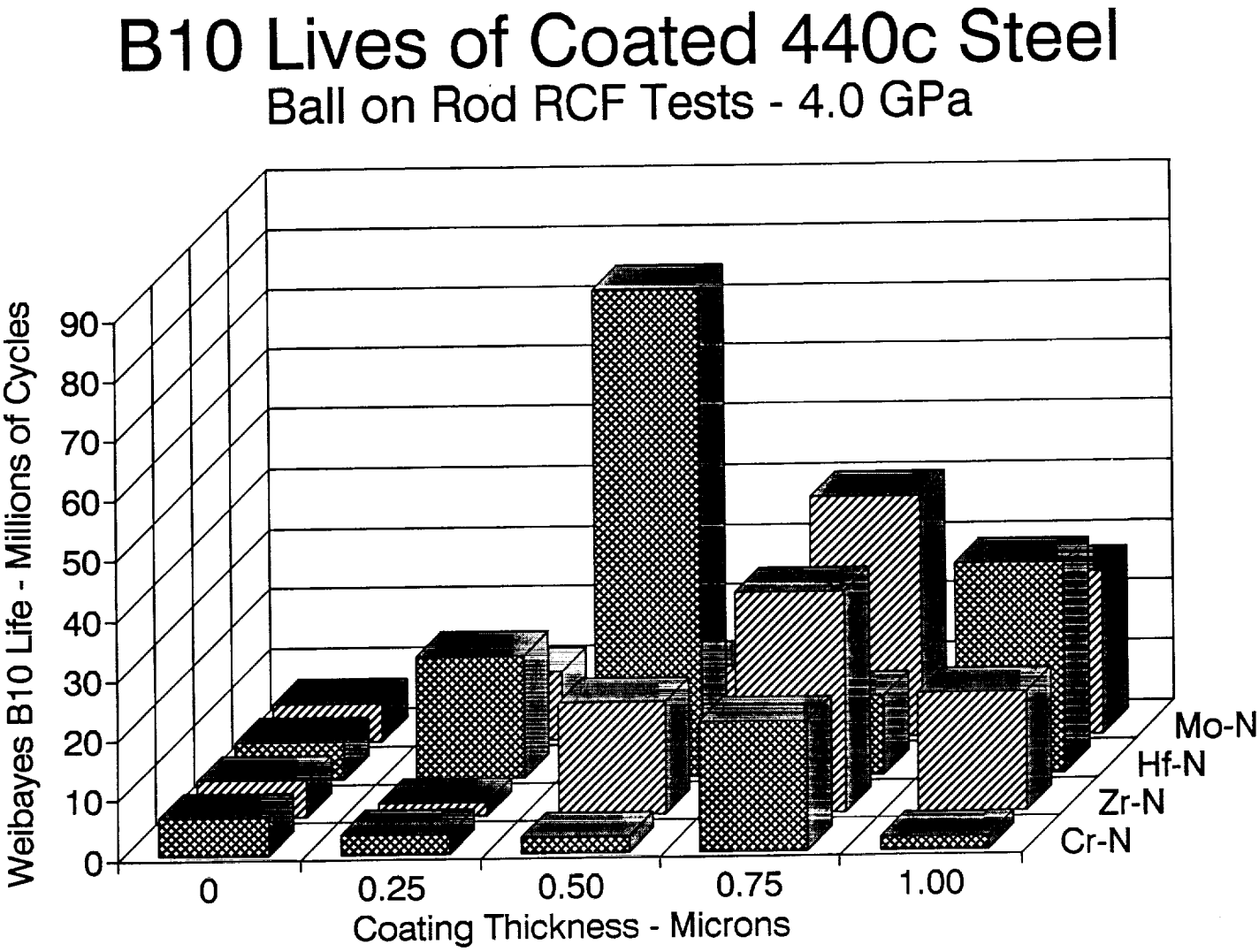

Figure 10. B10 lives of coated 440C stainless steel. Ball on rod RCF tests conducted at 4.0 GPa for the non-titanium compounds.

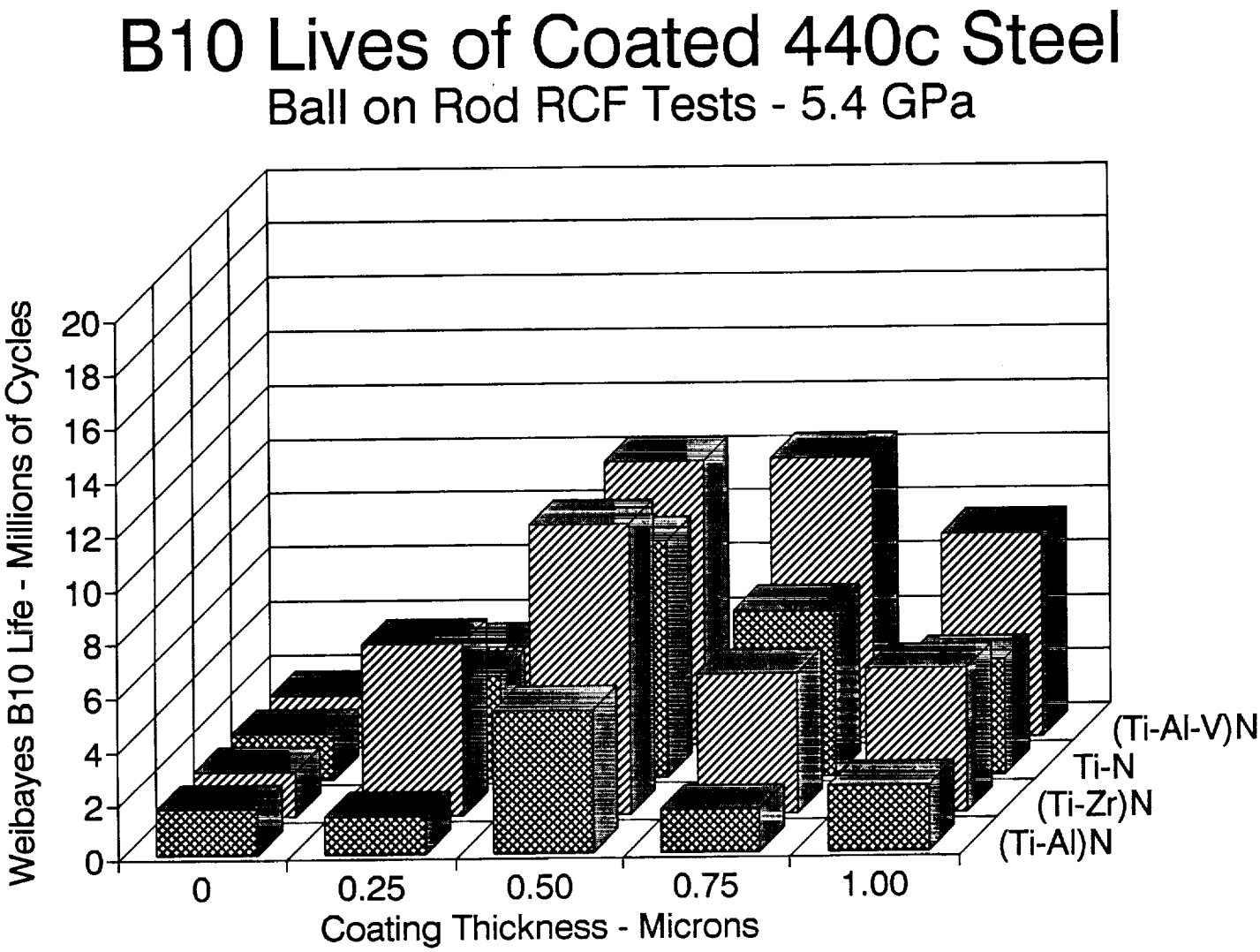

Figure 11. B10 lives of coated 440C stainless steel. Ball on rod RCF tests conducted at 5.4 GPa for the titanium compounds.

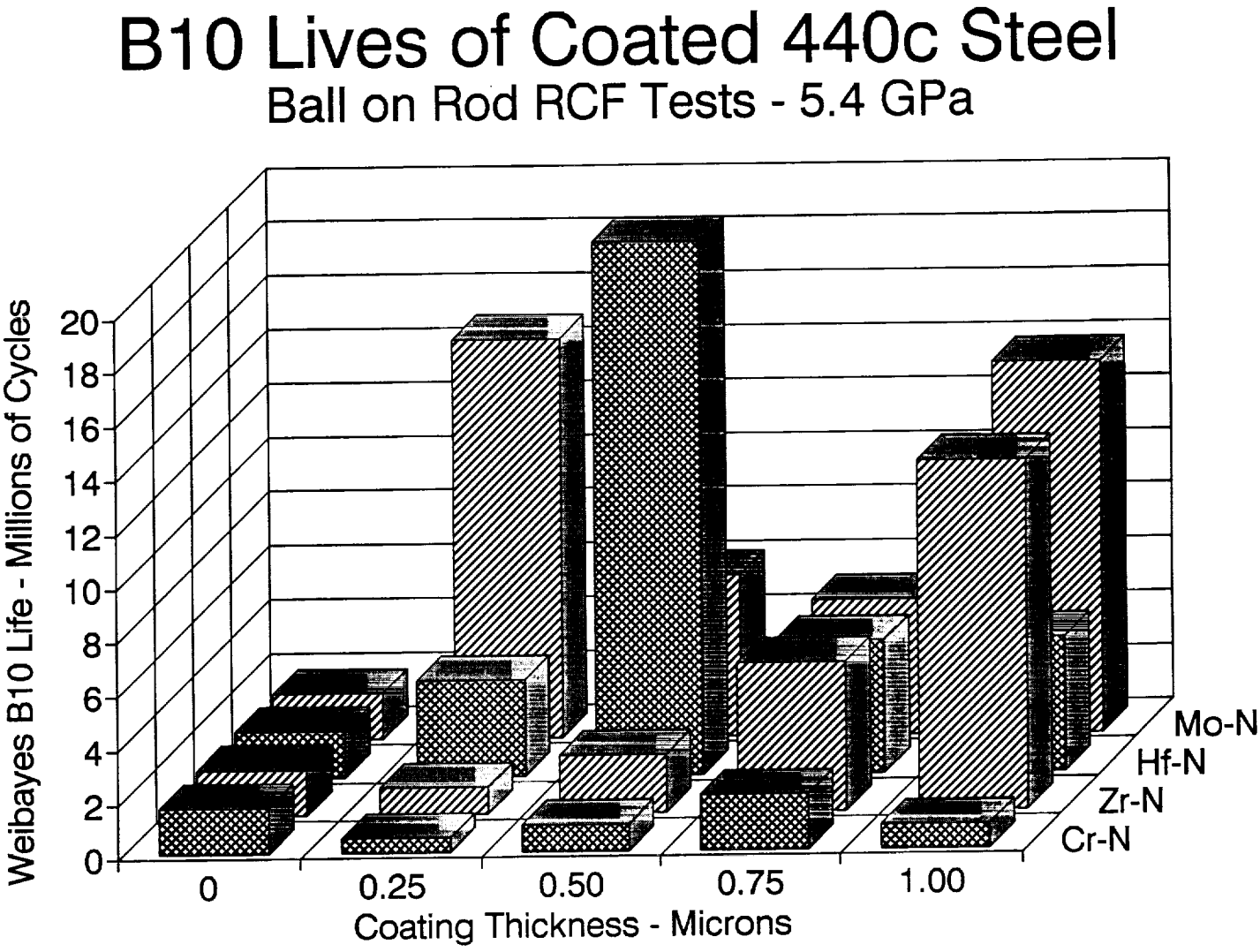

Figure 12. B10 lives of coated 440C stainless steel. Ball on rod RCF tests conducted at 5.4 GPa for the non-titanium compounds.

charts was selected for best viewing, and this order is maintained for both stress levels. The zero coating thickness (the uncoated rods) is the baseline for the tables and the charts. All eight of the coatings materials produced an improvement in the Weibayes B10 RCF life either at one or both of the stress levels. The best improvement in the Weibayes B10 life for all of the coatings came from the 0.5 μm thick HfN coating, which gave an improvement of 13 times at the 4.0 GPA stress and 12 times at the 5.4 GPa stress. All four HfN coating thicknesses gave an improvement in RCF life at both stress levels, but it was the 0.5 μm thick coatings that gave the best improvement by a large margin.

Two other nitride coatings, ß-Mo_2N and (Ti-Al-V)N also gave very good improvements in the RCF life at both stress levels for all four coating thicknesses, and TiN and $Ti_{0.5}Zr_{0.5}N$ gave improvements in the RCF life at both stress levels for seven of the eight coating thicknesses. ZrN worked well at both stress levels for 3 of the 4 coating thicknesses. Only the 0.25 μm thick ZrN coating did not produce an improvement in RCF life. In general, all of the titanium based materials with the exception of $Ti_{0.5}Al_{0.5}N$, gave good improvements in the RCF life.

Two of the eight nitride coatings produced only a marginal improvement. CrN gave only an improvement of 3.4 times over the baseline value for the 0.75 μm thick coating at the 4.0 GPa stress and 1.2 times at the 5.4 GPa stress, but all of the other thicknesses for CrN at both stress levels produced B10 lives that were less than the baseline value. The results were similar for $Ti_{0.5}Al_{0.5}N$, which only had an improvement in the B10 RCF life for the 0.5 μm thick coating at the 5.4 GPa stress level.

The peak in improvement in RCF life usually is found for specimens with coating thicknesses in the range of 0.5 to 0.75 μm. This generalization holds for the results from the tests conducted at the 4.0 GPa stress level and for the titanium based coatings at the 5.4 GPa stress level. For the ß-Mo_2N coating at the 5.4 GPa stress level, the highest improvements in RCF life were for the 0.25 and 1.0 μm thick coatings, both of which had about an 8 fold improvement in RCF life compared to an uncoated rod. The 0.5 and 0.75 μm

thick ß-Mo_2N coatings only had an improvement of about 3 times over an uncoated rod, which is good but not as good as the other thicknesses gave.

The tests of the ZrN coating at the 5.4 GPa stress level showed that the RCF life was improving with coating thickness. The thinnest ZrN coating tested at 5.4 GPa actually had a decrease in RCF life compared to an uncoated sample, but as the coating increased in thickness from 0.5 to 1.0 μm, the improvement in RCF life went from 1.3 to 3.3 to 7.7 times that of an uncoated sample. Since no coatings thicker than 1.0 μm were made, it is not known if thicker ZrN coatings would have continued the increase in RCF life. Prior work [32-34] with thick TiN coatings (2.5 and 5.0 μm) produced a decrease in RCF life [27], and it is felt that ZrN coatings with thicknesses much over 1 μm would also have a decrease in RCF life.

The residual stress in PVD hard coatings is usually highly compressive, and it is believed that it is this compressive stress that contributes greatly to the improvement in RCF life up to a certain coating thickness. Chang et al. [34] showed that the surface of an uncoated rolling element was plastically deformed and full of cracks after only 10 million cycles in an RCF test, whereas a 1.0 μm thick TiN coated specimen did not show any damage after 33 million cycles at the same load. The compressive stress in the thin coating prevented cracks from nucleating and propagating, but once the coating thickness exceeded 1 μm, the coated specimen did not perform as well as an uncoated one. The combined stress from the load and the residual stress caused the coating to spall, and the wear was accelerated with the very abrasive particles in the system.

Unbalanced magnetron sputtering produces high ion bombardment of the growing film, which improves both the hardness and the adhesion of the films. The ion bombardment also heats the film and substrate, and the goal is to achieve the best film properties without softening the substrate material. The 440C stainless steel used in this work begins to soften at 250°C, and the data given in Tables 4 and 5 show that there was in all cases some degree of softening of the substrate. This softening was not intentional, and in most cases it did not produce a detrimental effect. Additional work needs to be

done on controlling the temperature of sensitive substrate materials during unbalanced magnetron sputtering of hard coatings.

The largest drop in substrate hardness occurred for the substrates coated with CrN, and the performance of these coated samples was reduced by the softening of the substrate. If the substrate cannot support the coating, the brittle coating will crack and spall, which leads to early failure. Similar results can be seem for the $Ti_{0.5}Al_{0.5}N$ coated samples, which also were softened for the two thicker samples.

Softening of the substrate did not lead to poor performance in all cases. Some softening of the substrates occurred for both the TiN and (Ti-Al-V)N, but these coated samples did do better than uncoated ones, with the exception of the 0.25 μm thick TiN coating. It has been observed [50] on high speed steel cutting tools coated with TiN and HfN that the TiN coatings remained intact during the cutting process whereas the HfN coatings cracked and spalled off. During the high speed cutting process, the nose of the tool deformed due to the high load and temperature generated during cutting, but the TiN coating did not break up. It deformed along with the tool and remained in place as a barrier to wear. HfN on the other hand broke off and was not there to provide any protection.

The TiN and (Ti-Al-V)N coatings on the RCF test rods may be behaving in a similar manner as TiN does on cutting tools. The coating is flexible (on a relative scale), and if the substrate deforms, the coating deforms as well. It remains in place to do its job of extending the life of the coated surface.

Gold and Copper Coatings

The preliminary results of the RCF tests of the gold and copper coatings, some of which are still underway, are summarized in Table 6 and are shown graphically in Figure 13. RCF tests conducted up to the time of the writing of this report show that the Au and Cu metal films at the 5.4 GPa stress level provide no significant improvements in life for the 0.25, 0.50, and 0.75 μm coating thicknesses. Tests of specimens with the 1.0 μm thickness have not been started yet.

Table 6.
Preliminary Results of Rolling Contact Fatigue Tests for Gold and Copper Coatings

Rod Number	Coating		Weibayes B10 Life				Improvement factor over baseline		Rod Hardness, Rc		
	Material	Thick-ness, μm	Hours		10^6 Cycles		4.0 GPa	5.4 GPa	Before Coating	After Coating	Decrease
			4.0 GPa	5.4 GPa	4.0 GPa	5.4 GPa					
	Baseline	0	145.4	39.6	75.0	20.4	1.0	1.0	59.1	-	0
542	Au	0.25	*	35.7	*	18.4	*	0.9	57.0	57.0	0
517		0.50	*	22.4	*	11.6	*	0.6	56.8	56.8	0
519		0.75	*	53.8	*	27.8	*	1.4	56.9	56.9	0
518		1.00	*	*	*	*	*	*	57.0	56.9	0.1
496	$(Ti_{0.5}Al_{0.5})N$	0.25	*	37.0	*	19.1	*	0.9	57.0	56.3	0.7
498		0.50	*	74.8	*	38.6	*	1.9	57.1	56.1	1.0
449		0.75	*	50.7	*	26.2	*	1.3	56.6	56.6	0
447		1.00	*	*	*	*	*	*	55.9	55.5	0.4

* - Test in Progress

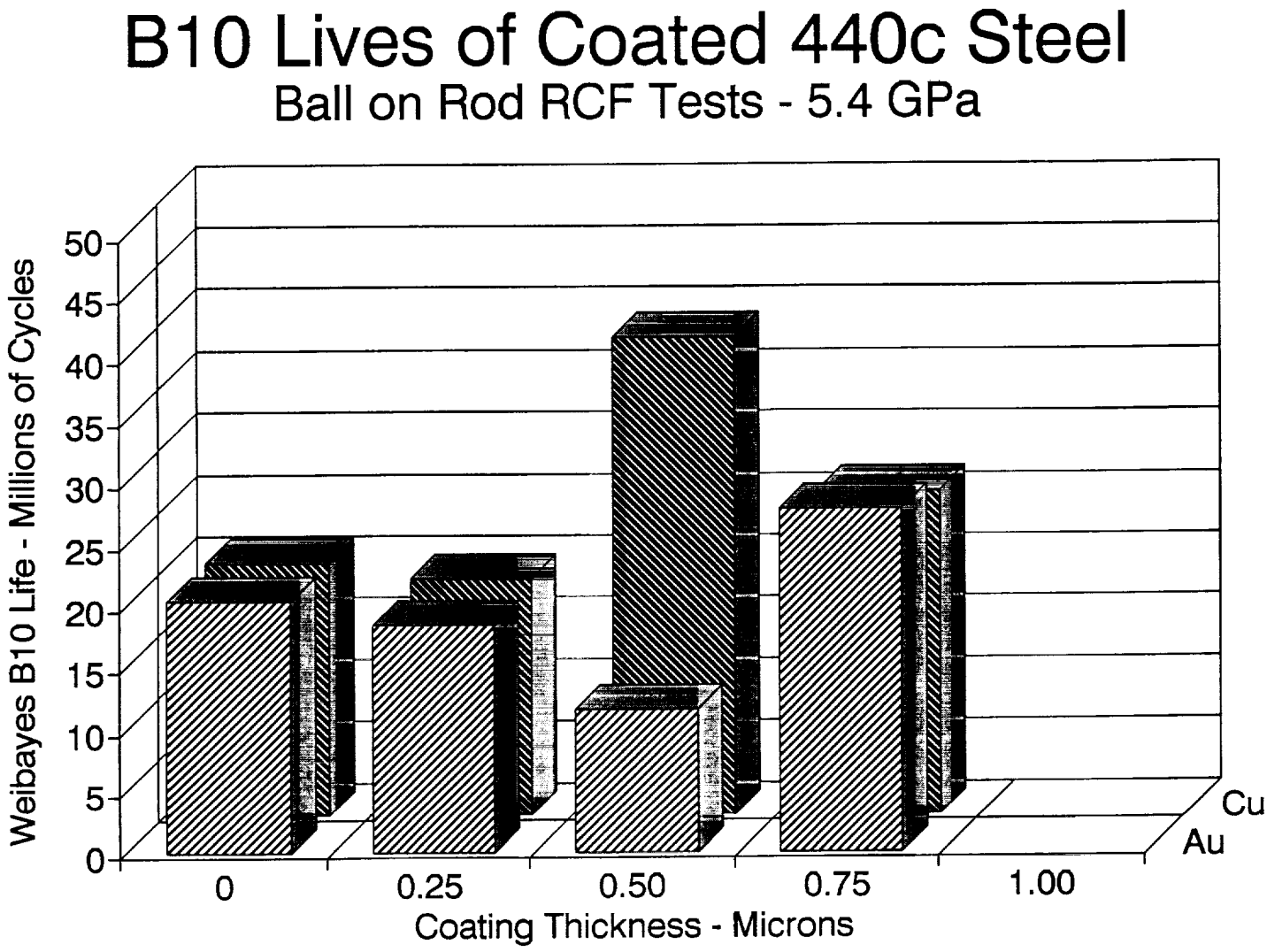

Figure 13. B10 lives of Au and Cu coatings on 440C stainless steel. Ball on rod RCF tests conducted at 5.4 GPa for the non-titanium compounds.

Although the RCF tests of the Au and Cu coatings at the 4.0 GPa stress level have not been completed yet, the preliminary results are indicating very large improvements in RCF life. It is anticipated that B10 lifetimes will be over an order of magnitude greater than the baseline. The eventual B10 lifetime will depend on how long the test is run before it is suspended or before a failure occurs. Individual tests are being allowed to run for several months in an effort to obtain an accurate and not overly conservative B10 lifetime.

OTHER RESULTS FROM THIS PROGRAM

When BIRL undertook this coating program for NASA MSFC, the importance of substrate ion bombardment was well understood by the BIRL researchers, and it was known that techniques to ensure high substrate ion bombardment in the then new opposed-cathode sputtering system would be necessary. It was fortuitous that the onset of the NASA program at BIRL occurred soon after the work by Window and Savvides [13-15]. The BIRL workers were able to learn from their publications, and they were quick to implement them. There was a need to supply additional substrate ion bombardment in the opposed-cathode system, and unbalanced magnetron sputtering was a possible means to meet this need. BIRL's early involvement with UBM sputtering has put BIRL in the forefront of this technology in the United States and in the world. Without NASA MSFC's early support for the hard coating program for bearing materials, BIRL would not have made such quick progress in the unbalanced magnetron technology.

This NASA MSFC coating program at BIRL also supported a Ph.D. graduate student, Suzanne L. Rohde, and she completed her doctoral work in December, 1991. The title of her thesis was "Metal-Nitride Thin Films Deposited by Unbalanced Magnetron Sputtering." Dr. Rohde is now an assistant professor in the Department of Materials Science and Engineering at the University of Nebraska, Lincoln. In addition to the thesis published by Dr. Rohde, a total of 19 papers have been written and published (or submitted for publication) on the work from this program. These papers are all listed in the References section, and they references 17, 19, 22, 24, 25, 41, 42, and 51-62.

FUTURE WORK

Our pioneering work with unbalanced magnetron sputtering has shown that it offers many advantages for depositing hard coatings onto steel substrates, including:

- High hardness, fully dense coatings
- Excellent adhesion of the coating to the substrate
- High deposition rates
- Excellent process reproducibility
- Controlled substrate coating temperature

Approach

Although the results from this NASA MSFC program at BIRL are very encouraging, there is still much work to be done in the area of hard coatings for bearing applications. To continue our effort, we recommend a multi-task program with five major tasks, which would be coating development, adhesion studies, sample preparation, characterization including tribological testing, and reporting.

Task 1

The first Task would involve an in-depth study of the effect of the process parameters on the properties of reactively deposited coatings such as CrN_x, $Ti_{0.5}Al_{0.5}N$, HfN, and the polycrystalline superlattice coating, TiN/NbN. This last coating is one that has been developed at BIRL over the past two years [63-65], and the main feature of this polycrystalline superlattice coating is that the hardness of the coating can be as high as 5200 kgf mm^{-2}. The first three coatings, CrN_x, $Ti_{0.5}Al_{0.5}N$, and HfN were chosen because of our prior experience with them under our NASA MSFC program. They have the potential to be very good tribological materials, but time did not permit us the opportunity to explore the full range of compositions and process parameters to find the best tribological material. The last coating, polycrystalline

superlattice TiN/NbN, is a very new materials that because of its high hardness may also potentially be a very good tribological coating.

Coatings would be prepared on 440C stainless steel and M2 tool steel substrates under different sputter etch, target power, total pressure, reactive gas partial pressure, substrate bias voltage, and substrate bias current density conditions, and the effect of these changes of process parameters on the coating structure and properties would be evaluated in the characterization task. Properties to be evaluated would be hardness, adhesion, composition, crystal structure, and coating morphology. In addition, for CrN_x, the effect of coating composition would also be evaluated. All of the work in the characterization phase would be done with the aid of statistically designed experiments to minimize the experimental time and to maximize the results.

The unbalanced magnetron sputtering systems offer a unique opportunity to independently control the ion flux during both sputter etching and deposition. This independent control has not been possible before with conventional magnetron sputtering systems. In the case of etching, the amount of ion flux at a given etching voltage will affect the adhesion of the coating and the temperature rise of the substrate. During deposition, the substrate bias voltage and ion flux density determine the structure and orientation of the coating, and there is a need for cross-section transmission electron microscopy (XTEM) and X-ray diffraction residual stress measurements on unbalanced magnetron hard coatings.

A primary concern in all of this work is the ability to reactively sputter deposit coatings on steel substrates without changing the metallurgical properties of the steel. In prior work, it has been demonstrated that it is possible to deposit coatings such as TiN onto common engineering alloys like 440C stainless steel without significantly softening the steel. If care was taken to heat sink the substrates, it was possible to have virtually no softening of the steel, but more work is needed in this area to expand the range of materials that can be worked with. As the process parameters are varied in the first task, the operating envelope for depositing the coatings

onto steels such as 440C stainless without reducing the hardness would be determined. Thermal management techniques for the substrate such as heat sinking and fixture design would be explored.

Although future work will involve the current 440C stainless steel substrate material, new bearing steel should also be considered. The 440C stainless steel has been chosen as a bearing steel partly for its corrosion resistance. Even though the 440C stainless steel is hardenable, it does not reach the hardness and strength of other alloy steels. The nitride coatings are very corrosion resistant, and they can provide the corrosion protection for the steel substrate. It would then be possible to consider other steels such as M50 alloy steel or other high strength steels such as the new bearing materials under development as the base material. Any future work coating work should definitely include other steel substrate materials in addition to the 440C stainless steel.

Task 2

The second task would involve a separate study of the effect of process parameters on the adhesion of the coating to the substrate. The critical load for adhesion of a hard coating on a steel substrate, as measured by the scratch test, is a function of several factors including the substrate hardness, coating thickness, residual stress, and the thermal expansion match between the substrate and coating. For a given coating thickness, the critical load will increase as the substrate hardness increases.

Recently at BIRL, it has been shown that it is possible to increase the critical load for hard coatings on relatively soft substrates to values that are normally found for hard substrates. This finding is particularly important for stainless steel substrates that cannot achieve the same high hardness as a tool steel. The second task then would look at the effect of substrate bias voltage on the critical scratch test load of the coating and would determine ways to maximize the critical load for a particular substrate/coating combination.

Task 3

The third task would be the preparation of coated samples for tribological testing at BIRL. Statistically designed experiments would be used to aid in the correlation of process parameters and coating structure to the performance of the coatings in such tribological tests as rolling contact fatigue, traction, or pin-on-disk. BIRL would perform one or more of these tribological tests in order to have an in-house feedback on the tribological performance of the coatings. If a teaming arrangement could be set up, additional tribological tests could be carried out by team members.

Task 4

The coatings produced in such a program would be characterized in the fourth task. Selected samples of each of the coatings would be characterized with both micro- and nano-indentation hardness tests, scratch adhesion tests, tribological tests, scanning and cross-section transmission electron microscopies, X-ray diffraction, and Auger electron spectroscopy. All of the characterization would be done to correlate the properties of the coatings to the process parameters.

Task 5

The fifth task would be the reporting phase of the program. The frequency of the reports would be dictated by the sponsor, but it is expected that reports would be written at least on a semi-annual basis.

BIRL strongly recommends that the program on coatings for bearing applications be continued to take advantage of what has already been learned and to try to solve some of the outstanding problems that were discovered in the initial work. Much progress has been made, but it is safe to say that much more can be discovered if the program were to continue.

SUMMARY

The results from this program have been outstanding. Eight different nitride coatings and two pure metal coatings have been successfully deposited on 440C stainless steel substrates, for the most part without significantly changing the metallurgical properties of the steel. The nitride coatings have extended the rolling contact fatigue life of the coated samples by many times the life of an uncoated sample, and the greatest improvement in RCF life was for the 0.5 μm thick HfN coating, which produced an improvement of 12 to 13 times for each of the two test loads. This work has shown that it is definitely possible to improve the rolling contact fatigue life of rolling elements by applying a thin, hard coating to them, and the technology developed in this program should be applied to high speed rolling element bearings. Over the 3 years of this program, the unbalanced magnetron sputtering technology has been developed and commercialized. It is now possible to go to suppliers and have these coatings done commercially in unbalanced magnetron units.

REFERENCES

1. "Application of Hard Coatings to Substrates at Low Temperatures," program sponsored by the National Aeronautics and Space Administration, Marshall Space Flight Center, Contract number, NAS 8-37686.

2. W. D. Sproul, Thin Solid Films, 107 (1983) 141.

3. W. D. Sproul, "Wear of Sputter Deposited Refractory-Metal Nitride Coatings," W. D. Sproul, J. E. Greene and J. A. Thornton (eds.), in Physics and Chemistry of Protective Coatings, American Institute of Physics, Conf. Proc. 149, New York, 1986, p. 157.

4. W. D. Sproul, Surf. Coat. Technol., 33(1) (1987) 73.

5. W. D. Sproul and J. R. Tomashek, "Rapid Rate Reactive Sputtering of a Group IVB Metal," U. S. Patent 4,428,811, January 31, 1984.

6. W.-D. Münz, D. Hofmann, K. Hartig, Thin Solid Films, 96 (1982) 79.

7. W.-D. Münz, J. Vac. Sci. Technol. A, 4(6) (1986) 2717.

8. D. G. Teer, Surf. Coat. Technol., 39/40 (1989) 565.

9. W.-D. Münz, Surf. Coat. Technol., 48 (1991) 81.

10. W. D. Sproul, P. J. Rudnik, C. A. Gogol, and R. Mueller, Surf. Coatings Technol., 39/40 (1989) 499.

11. W. D. Sproul, P. J. Rudnik, and C. A. Gogol, R&D Magazine, November 1989, 79.

12. J. J. Cuomo and S. M. Rossnagel, J. Vac. Sci. Technol. A, 4(3) (1986) 393.

13. B. Window and N. Savvides, J. Vac. Sci. Technol. A, 4(2) (1986) 196.

14. B. Window and N. Savvides, J. Vac. Sci. Technol. A, 4(3) (1986) 453.

15. N. Savvides and B. Window, J. Vac. Sci. Technol. A, 4(3) (1986) 504.

16. J. Musil and S. Kadlec, Vacuum, 40(5) (1990) 435.

17. S. L. Rohde, W. D. Sproul, and J. R. Rohde, J. Vac. Sci. Technol. A, 9(3), 1178 (1991).

18. H. Freller and H. P. Lorenz, J. Vac. Sci. Technol. A, 4(6) (1986) 2691.

19. S. L. Rohde, I. Petrov, W. D. Sproul, S. A. Barnett, P. J. Rudnik, and M. E. Graham, Thin Solid Films, 193/194 (1990) 117.

20. D. G. Teer, Surf. Coat. Technol., **35** (1988) 901.

21. W.-D. Münz, D. Schulze, and F. J. M. Hauzer, Surf. Coat. Technol., **50** (1992) 169.

22. William D. Sproul, Paul J. Rudnik, Michael E. Graham, and Suzanne L. Rohde, Surf. Coat. Technol., **43/44** (1990) 270.

23. S. L. Rohde, L. Hultman, M. S. Wong, W. D. Sproul, and J. R. Rohde, Surf. Coat. Technol., **50** (1992) 255.

24. M.-S. Wong, W. D. Sproul, and S. L. Rohde, Surf. Coat. Technol., **49** (1991) 121.

25. J. F. Dill, M. N. Gardos, H. E. Hintermann, and H. J. Boving, ASLE Proceedings, 3rd International Conference on Solid Lubrication, ASLE-SP-14, 1984, p. 230.

26. R. F. Hochman, A. Erdemir, F. J. Dolan, and R. L. Thom, J. Vac. Sci. Technol. A, **3** (1985) 2348.

27. R. L. Thom, A. Erdemir, and R. F. Hochman, in R. F. Hochman (ed.), Proceedings Conference Ion Plating and Implantation; Applications to Materials, ASM Metals Park, OH, 1986, p. 183.

28. A. Erdemir and R. F. Hochman, Surf. Coat. Technol., **36** (1988) 755.

29. A. Erdemir and R. F. Hochman, in R. F. Hochman, H. Legg, and K. O. Legg (Eds.), Proceedings Conference on Ion Implantation and Plasma Assisted Processes for Industrial Applications, ASM, Metals Park, OH, 1988, p. 43.

30. A. Erdemir, "A Study of Surface Metallurgical Characteristics of TiN Coated Bearing Steels," Ph.D. Thesis, Georgia Institute of Technology, Atlanta, GA, 1986.

31. A. Erdemir, Surf. Coat. Technol., **54/55** (1992) 482.

32. H. S. Cheng, T. P. Chang, and W. D. Sproul, Proceedings 16th Leeds/Lyon Conference on Tribology, 1989, Tribology Series 17, Elsevier, Amsterdam, 1990, p. 81.

33. T. P. Chang. H. S. Cheng, and W. D. Sproul, Surf. Coat. Technol., **43/44** (1990) 699.

34. T. P. Chang. H. S. Cheng, W. A. Chiou, and W. D. Sproul, Tribol. Trans., **34** (1991) 408.

35. W. D. Sproul, P. J. Rudnik, M. E. Graham, C. A. Gogol, and R. M. Mueller, Surf. Coat. Technol. **39/40** (1989) 499.

36. W. D. Sproul, J. Vac. Sci. Technol., **4(6)** (1986) 2874.

37. G. Håkansson, J.-E. Sundgren, D. McIntyre, J. E. Greene, and W.-D. Münz, Thin Solid Films, **153** (1987) 55.

38. D. McIntyre, J. E. Greene, G. Håkansson, J.-E. Sundgren, and W.-D. Münz, J. Appl. Phys., **67(3)** (1990) 1542.

39. O. Knotek, M. Atzor, and H.-G. Prengel, Surf. Coat. Technol., **36** (1988) 265.

40. W.-D. Münz, J. Vac. Sci. Technol. A, **4** (6) (1986) 2717.

41. M. E. Graham, P. J. Rudnik, and W. D. Sproul submitted to Surface and Coatings Technology for publication.

42. P. J. Rudnik, M. E. Graham, and W. D. Sproul, Surf. Coat. Technol., **49** (1991) 293.

43. JCPDS X-ray index cards 38-1420, 35-753, 33-592, and 11-65 for TiN, ZrN, HfN, and CrN, respectively.

44. O. Knotek, W. Bosch, W.-D. Münz, Proc. 11th Plansee Conference, Vol. 1, Reutte, Austria (1985), p. 605.

45. JCPDS X-ray index card 24-768 for ß-Mo_2N.

46. A. J. Perry, A. W. Baouchi, J. H. Petersen, and S. D. Pozder, Surf. Coat. Technol., **54/55** (1992) 261.

47. O. Knotek, M. Böhmer, and T. Leyendecker, J. Vac. Sci. Technol. A, **4(6)** (1986) 2695.

48. D. Glover, in J. J. C. Hoo (Ed.), Rolling Contact Fatigue Testing of Bearing Steels, ASTM STP 771, 1982, p. 107.

49. R. B. Abernathy, J. E. Breneman, C. H. Medlin, and G. L. Reinman, "Weibull Analysis Handbook," AFWAL-TR-83-2079, Wright Aeronautical Laboratories, WPAFB, Ohio, November 1983, p. 67.

50. G. R. Fenske, N. Kaufherr, R. H. Lee, B. M. Kramer, R, F, Bunshah, and W. D. Sproul, Surf. Coat. Technol., **36** (1988) 791.

51. William D. Sproul, NASA Conference Proceedings 3092, Vol. II, Advanced Earth-to-Orbit Propulsion Technology 1990, George C. Marshall Space Flight Center, Marshall Space Flight Center, Alabama, May 15-17, 1990, pp. 555-564.

52. D. S. Stone, K. B. Yoder, and W. D. Sproul, J. Vac. Sci. Technol. A. 9(4), (1991) 2543.

53. W. D. Sproul, Surf. Coat. Technol., **49** (1991) 284.

54. W. D. Sproul, T. P. Chang, and H. S. Cheng, Proceedings of the 1991 Automotive Technology Development Contractors' Coordination Meeting, Dearborn, MI, October 28-31, 1991, pp. 567-569.

55. S. L. Rohde, A. J. Nelson, A. Mason, and W. D. Sproul, J. Vac. Sci. Technol. A., 10(4) (1992) 1797.

56. William D. Sproul, 35th Annual Technical Proceedings, Society of Vacuum Coaters Meeting, Baltimore, MD, March 22-27, 1992. p. 236.

57. William D. Sproul, Proceedings of the 11th International Conference on Vacuum Metallurgy, Antibes, France, May 11-14, 1992, published in Supplément Revue "Le Vide, les Couches Minces N° 261 - Mars-Avril 1992, pp. 183-190.

58. K. Yoder, D. S. Stone, W. D. Sproul, and P. J. Rudnik, submitted for publication in the Proceedings of the 1992 Conference on Advanced Earth-to-Orbit Propulsion Technology, held at the George C. Marshall Space Flight Center, Marshall Space Flight Center, Alabama, May 20, 1992.

59. William D. Sproul, submitted for publication in the Proceedings of the 1992 Coatings for Advanced Heat Engines Workshop, held at the Naval Postgraduate School, Monterey, CA, August 3-6, 1992.

60. William D. Sproul, accepted for publication in the proceedings of the 12th International Vacuum Congress, The Hague, The Netherlands, October 12-16, 1992 to be published in Materials Science and Engineering.

61. Robert Thom, Lewis Moore, William D. Sproul, and T. Peter Chang, submitted for publication in Thin Solid Films or Surface and Coatings Technology (Proceedings ICMCTF 93).

62. William D. Sproul, Michael E. Graham, Ming-Show Wong, and Paul E. Rudnik, submitted for publication in Surface and Coatings Technology (Proceedings ICMCTF 93).

63. X. Chu, M. S. Wong, W. D. Sproul, S. L. Rohde, and S. A. Barnett, J. Vac. Sci. Technol. A. 10(4), (1992) 1604.

64. X. Chu, M. S. Wong, W. D. Sproul, and S. A. Barnett, submitted for publication in Surface and Coatings Technology.

65. X. Chu, M. S. Wong, W. D. Sproul, and S. A. Barnett, Mat. Res. Soc. Symp. Proc., Vol. 286, 1993, p. 379.

BIRL:
Its Mission and Research Focus

BIRL is the industrial research laboratory at Northwestern University. BIRL performs applied research and development work directed toward technology transfer and commercialization. BIRL conducts, under proprietary and non-proprietary contract, a wide variety of programs on materials development, processing, and characterization for small and large industrial firms, associations, and government agencies.

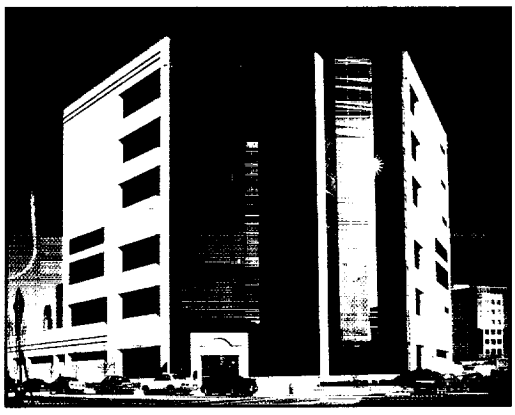

BIRL

1801 Maple Avenue
Evanston, Illinois 60201-3135

(708) 491-7600
FAX (708) 491-4486